The giant Chalukou porphyry Mo deposit, NE China: The product of a short-lived, high flux mineralizing event

Qingqing Zhao[1], Degao Zhai[1*], Ryan Mathur[2], Jiajun Liu[1], David Selby[3, 4], Anthony E. Williams-Jones[5]

[1]*State Key Laboratory of Geological Processes and Mineral Resources, China University of Geosciences, Beijing, 100083, China*

[2]*Department of Geology, Juniata College, Huntingdon, PA 16652, USA*

[3]*Department of Earth Sciences, Durham University, Durham, DH1 3LE, UK*

[4]*State Key Laboratory of Geological Processes and Mineral Resources, School of Earth Resources, China University of Geosciences, Wuhan, 430074, China*

[5]*Department of Earth and Planetary Sciences, McGill University, Quebec, H3A 0E8, Canada*

[*]E-mail: dgzhai@cugb.edu.cn

Revised submission to: *Economic Geology*

With 29 pages, 9 Figures and 3 Tables

9-Nov-2020

Abstract

Whether giant porphyry ore deposits are the products of single short-lived magmatic-hydrothermal events or multiple events over a prolonged interval is a topic of considerable debate. Previous studies, however, have all been devoted to porphyry Cu and Cu-Mo deposits. In this paper, we report high-precision isotope dilution-negative-thermal ionization mass spectrometric (ID-N-TIMS) molybdenite Re-Os ages for the newly-discovered, world-class Chalukou porphyry Mo deposit (reserves of 2.46 Mt @ 0.087 wt.% Mo) in northeast (NE) China. Samples were selected based on a careful evaluation of the relative timing of the different vein types (i.e., A, B and D veins), thereby ensuring that the suite of samples analyzed could be used to reliably determine the age and duration of mineralization.

The molybdenite Re-Os geochronology reveals that hydrothermal activity at Chalukou involved two magmatic-hydrothermal events spanning an interval of 6.92 ± 0.16 m.y.. The first event (153.96 ± 0.08/0.63/0.79 Ma, molybdenite ID-N-TIMS Re-Os age) was associated with the emplacement of a granite porphyry dated at 152.1 ± 2.2 Ma (zircon LA-ICP-MS U-Pb ages), and led to only minor Mo mineralization, accounting for <10% of the overall Mo budget. The bulk of the Mo (>90 %) was deposited in less than 650 Ka, between 147.67 ± 0.10/0.60/0.76 and 147.04 ± 0.12/0.72/0.86 Ma (molybdenite ID-N-TIMS Re-Os ages), coincident with the emplacement of a fine-grained porphyry at 148.1 ± 2.6 Ma (zircon LA-ICP-MS U-Pb ages). The high-precision Re-Os age determinations presented here show, contrary to the finding of a number of studies of porphyry Cu and Cu-Mo systems, that the giant Chalukou porphyry Mo deposit primarily formed in a single, short-lived (<650 Ka) hydrothermal event, suggesting that this may also have been the case for other giant porphyry Mo deposits.

Introduction

In recent years, numerous studies have been devoted to determining the age and duration of magmatic-hydrothermal processes in porphyry ore systems, e.g., the El Teniente Cu-Mo porphyry deposit, Chile (Maksaev et al., 2004; Spencer et al., 2015), the Tibetan Qulong porphyry Cu-Mo deposit, China (Li et al., 2017a, b), and the Bajo de la Alumbrera porphyry Cu-Au deposit, Argentina (von Quadt et al., 2011). As multiple intrusions are common in porphyry systems, many of these studies have suggested that giant porphyry Cu deposits form over long periods of time as the

products of multiple, albeit short-lived (<100,000 years), magmatic-hydrothermal events separated by long intervals of quiescence (e.g., Carten et al., 1988; Cathles et al., 1997; Mathur et al., 2000; Cook et al., 2005; Braxton et al., 2012; Deckart et al., 2012, 2014; Weis et al., 2012; Stein, 2014; Mercer et al., 2015; Spencer et al., 2015; Weis, 2015). Some studies, however, have called on a single magmatic event of limited duration to explain the mineralization (von Quadt et al., 2011; Buret et al., 2016). Thus, whether all or even most giant porphyry deposits are the products of multiple mineralizing events associated with multiple intrusions (e.g., repetitive A-B-D veins) or single events related to a single intrusion remains unclear. This is particularly the case for giant porphyry Mo deposits, which have been the subject of far fewer detailed geochronological studies than porphyry Cu or Cu-Mo deposits (Selby and Creaser, 2001; Spencer et al., 2015).

With recent advances in radiometric dating methods, e.g., isotope dilution-negative-thermal ionization mass spectrometric (ID-N-TIMS) molybdenite Re-Os geochronology (Creaser et al., 1991; Selby and Creaser, 2001; Stein et al., 2001, 2003; Dilles et al., 2003; Morelli et al., 2010; Deckart et al., 2012; Lawley and Selby, 2012; Stein, 2014; Li et al., 2017b; Chang et al., 2017; Zhai et al., 2019a, 2020), it is now possible to obtain high-precision (‰ level) ages of individual vein types and establish a robust temporal relationship for the different vein stages that constitute porphyry deposits (e.g., Creaser et al., 1991; Selby and Creaser, 2001; Markey et al., 2007; Selby et al., 2007; Chiaradia et al., 2009a, b, 2013, 2014; Spencer et al., 2015; Chang et al., 2017). Consequently, we can now rigorously assess whether a particular porphyry deposit formed during a single magmatic-hydrothermal event or was the product of multiple such events.

The newly-discovered Chalukou porphyry Mo deposit in northeast (NE) China, with reserves of more than 2.46 million metric tons (Mt) Mo at an average grade of 0.087 wt.% Mo (Fig. 1; Nie et al., 2011; Li et al., 2014, 2019; Liu et al., 2014b), is one of the World's largest Mo deposits (for example, Climax contains 2.2 Mt Mo, Audétat, 2015, and Henderson contains 1.2 Mt Mo, Seedorff and Einaudi, 2004) and thus an excellent subject for a study designed to determine whether a giant porphyry Mo deposit can form in a single mineralizing event. This deposit is located in the Great Hingan Range metallogenic belt, which also hosts numerous porphyry Mo(-Cu), skarn Fe, epithermal Au-Ag and polymetallic (Ag-Pb-Zn) vein deposits (Dai et al., 2006, 2009; Chen et al., 2012, 2017; Zhai et al., 2014, 2017, 2019b; Gao et al., 2016; Shu et al., 2016). Observations of drill core show that the Chalukou Mo mineralization is mainly hosted by local granite porphyry, quartz

87 porphyry, and fine-grained porphyry, all of which experienced intense hydrothermal alteration (Nie
88 et al., 2013; Li et al., 2014). In principle, any or even all of these intrusions could have released the
89 fluids that formed the deposit. Thus, it is necessary to reconstruct the vein paragenesis, determine
90 the relationships of the different mineralized vein types to the different intrusions, and undertake
91 high precision dating of the different intrusions and associated molybdenite-quartz veins. Although
92 several geochronological studies have been conducted at Chalukou (Li et al., 2014; Liu et al., 2014b;
93 Zhang and Li, 2017; Duan et al., 2018), these studies did not establish the relative chronology of
94 the molybdenite-quartz veins that were dated and were restricted to samples from the deepest part
95 (>700 m) of the deposit, thereby limiting their application in quantitatively interpreting the history
96 of mineralization.
97 In this study, we made use of detailed drill core logging and thin section petrography to relate the
98 different vein types and associated alteration to specific intrusions, LA-ICP-MS zircon U-Pb
99 analyses to determine the ages of the three intrusions, and high-precision ID-N-TIMS molybdenite
100 Re-Os analyses to determine the ages of the different mineralized veins. Based on the results of this
101 study, we were able to interpret the absolute age and duration of Mo mineralization in the Chalukou
102 deposit and propose that the bulk of the Mo mineralization is temporally related to the emplacement
103 of the fine-grained porphyry. Consequently, we are able to show that multiple mineralization events
104 were, indeed, not responsible for the formation of this giant Mo deposit. Instead, most of the Mo
105 mineralization was due to the emplacement of a single intrusion and formed in <650 Ka.

106 **Ore Deposit Geology**

107 The Chalukou porphyry Mo deposit is located 80 km north of Jiagedaqi in Heilongjiang province
108 (E123° 49′ 15″ to E123° 56′ 30″ and N51° 08′ 15″ to N51° 11′ 00″), NE China. Geologically, this
109 part of China comprises the Erguna, Hingan, Songliao, and Jiamusi blocks (Fig. 1A; Wang et al.,
110 2011; Wu et al., 2011; Meng et al., 2011) and has undergone three stages of tectonic evolution since
111 the Proterozoic (Fu et al., 2011; Nie et al., 2011, 2013), involving the Paleo-Asian Ocean, the
112 Mongol-Okhost Ocean, and the Paleo-Pacific Ocean, respectively (Wu et al., 2005, 2011; Wilde,
113 2015; Zhou et al., 2018). During the Paleozoic, the tectonics of NE China were dominated by the
114 southward subduction of the Paleo-Asian Ocean, and several microcontinental blocks, namely the
115 Lesser Hingan, Jiamusi and Songliao blocks, were assembled along the Xilamulun fault (Chen et

al., 2017). In the Mesozoic, subduction of the Mongol-Okhotsk and Paleo-Pacific oceanic plates led to the emplacement of large volumes of granitic rocks and the development of a number of NE-striking faults. These granites, which include early Jurassic magmatic-arc granites and late Jurassic to early Cretaceous highly fractionated granites, formed large batholiths (Liu et al., 2017; Duan et al., 2018). The continental basement of NE China is exposed mainly at Liaoning and Hebei provinces, and is composed of Precambrian metamorphic rocks including amphibolites, schists, and marbles.

Numerous porphyry, skarn, and quartz vein-type Mo(-Cu) deposits have been discovered in NE China (Fig. 1B; Nie et al., 2007; Chen et al., 2012, 2017; Qin et al., 2017). This includes at least 78 Mo-bearing deposits (Chen et al., 2017) with a total Mo reserve of 10.5 Mt, among which the Chaluku deposit is the largest (2.46 Mt Mo @0.087 wt.%). Other notable deposits in NE China are the Caosiyao porphyry Mo deposit (2 Mt Mo @0.08 wt.%, Wang et al., 2017), the Daheishan porphyry Mo-Cu deposit (1.09 Mt Mo @0.066 wt.%, Wang et al., 2009) and the Luming porphyry Mo deposit (0.8 Mt Mo @0.088 wt.%, Hu et al., 2014). Owing to extensive dating of these deposits, the Mo mineralization has been shown to have developed during four distinct periods, i.e., 250-200, 200-160, 160-130, and 130-110 Ma (Chen et al., 2017). The 250-200 Ma Mo mineralization is mainly distributed in the northern part of the North China Craton (NCC) and is thought to be related to granites produced as a result of collision between the NCC and Siberia Craton (Chen et al., 2012, 2017; Wilde, 2015). The subduction of Mongol-Okhotsk and Paleo-Pacific plates led to the granitic magmatism responsible for the 200-160 and 160-130 Ma Mo mineralization, respectively (Chen et al., 2017). However, widespread late Jurassic arc magmatic rocks in the northern Great Hingan Range indicate that the subduction of the Mongol-Okhotsk Ocean may have lasted until 130 Ma (Duan et al., 2018). This was followed by roll-back of the Paleo-Pacific oceanic plate, which produced an extensional tectonic setting and is associated with felsic magmatism that is related to the known Mo mineralization dated between 130 to 110 Ma (Wu et al., 2005, 2011).

The Chalukou deposit is associated with granites that were emplaced during subduction of the Mongol-Okhotsk oceanic plate and has been subdivided into eastern and western exploration zones, which are separated by the Duobukuer River (Fig. 2A; Xiong et al., 2015). Exploration, however, has focused mainly on the eastern zone, which hosts the bulk of the currently known Mo resource (Meng et al., 2011). The Chalukou Mo mineralization in this zone is hosted by fine-grained porphyry,

146 granite porphyry, quartz porphyry, monzogranite and breccia pipes of Jurassic age and Lower
147 Ordovician volcanic rocks comprising rhyolite, rhyolitic tuff, dacite and andesite (Fig. 2B). The
148 main hosts to the mineralization, however, are the Ordovician volcanic rocks, which are also the
149 host to the granite porphyry, quartz porphyry and fine-grained porphyry (Fig. 3A). Cretaceous
150 diorite and monzonite porphyry dikes also were emplaced in the Ordovician volcanic rocks. The
151 other rocks in the eastern exploration zone are late Jurassic to early Cretaceous rhyolite and
152 Neoproterozoic quartz-chlorite schist, meta-sandstone, quartz-biotite schist, and minor marble (Fig.
153 2B). A set of ring fractures centered on the late Jurassic to early Cretaceous rhyolite predated the
154 mineralization and NE- and NW-striking faults post-dated it (Fig. 2A). The Mo mineralization has
155 been subdivided into a thin, upper low-grade (<0.06 wt.% Mo) zone and a lower, high-grade (0.08–
156 0.53 wt.%) zone (Nie et al., 2011; Zhang and Li, 2017), which passes upwards into a zone of
157 subordinate Pb-Zn epithermal mineralization. The western exploration zone is underlain mainly by
158 monzogranite and late Jurassic to early Cretaceous rhyolite. Quartz diorite is also exposed in this
159 zone.

160 Intrusive rocks in the district have been subdivided into three distinct stages based on detailed
161 drill core logging, namely pre-ore monzogranite, syn-ore fine-grained porphyry, granite porphyry
162 and quartz porphyry, and post-ore quartz monzonite porphyry and diorite porphyry (Figs. 2B, 3A).
163 The pre-ore monzogranite forms a batholith, which is exposed over an area of > 80 km^2 to the
164 northwest and southeast of the deposit (Nie et al., 2011; Liu et al., 2014a, 2015). In addition,
165 monzogranite is observed at depths of > 600 m below the southeast part of the Chalukou deposit,
166 where it intruded Ordovician volcanic rocks (Fig. 3A). The monzogranite is cut by fine-grained
167 porphyry and quartz monzonite porphyry, which are not exposed on the surface.

168 The granite porphyry and quartz porphyry were emplaced in the Ordovician volcanic rocks and
169 monzogranite batholith as dikes or small stocks with widths ranging from 3 to 80 m, whereas the
170 fine-grained porphyry, which is exposed only at a depth of 600 m below the surface, is a mushroom-
171 shaped intrusion that reaches a maximum width of 1000 m in the center of the Ordovician volcanic
172 rock unit (Fig. 3A). Mineralogically, the granite porphyry is composed of phenocrysts (2-5 mm) of
173 quartz (~12 vol.%), K-feldspar (~10 vol.%), and plagioclase (~4 vol.%) and minor biotite in a matrix
174 (~75 vol.%) of quartz and plagioclase. Accessory minerals include zircon, titanite and magnetite.
175 The quartz porphyry is compositionally similar to the granite porphyry and consists mainly of quartz

(~10 vol.%) and lesser proportions of plagioclase phenocrysts (1-3 mm, ~15 vol.%) in a matrix (~85 vol.%) of quartz and minor plagioclase. The fine-grained porphyry is composed of 1-2 mm diameter phenocrysts of K-feldspar (~5 vol.%), and quartz (< 1 vol.%) in a groundmass (~95 vol.%) dominated by quartz containing minor K-feldspar and plagioclase. The accessory minerals are magnetite, zircon and apatite. Unidirectional solidification textures (USTs) are observed in the apical part of the fine-grained porphyry intrusion, and are interpreted to record the transition from magmatic to hydrothermal conditions (Jin et al., 2014).

Previous geochronology

Previous studies have applied both zircon U-Pb (LA-ICP-MS) and molybdenite Re-Os (ICP-MS) methods to constrain the timing of magmatism and Mo mineralization at Chalukou (e.g., Nie et al., 2011; Li et al., 2014; Liu et al., 2014b; Liu et al., 2017; Zhang and Li, 2017). Zircon U-Pb dating of the granite porphyry yielded weighted mean $^{206}Pb/^{238}U$ ages ranging from 154.0 ± 1.0 to 149.0 ± 4.6 Ma (Li et al., 2014; Liu et al., 2014b; Zhang and Li, 2017; Duan et al., 2018). The quartz porphyry has been dated at between 148.0 ± 2.0 and 147.3 ± 1.5 Ma (Li et al., 2014; Liu et al., 2014b) and the fine-grained porphyry at between 148.0 ± 1.0 and 147.9 ± 1.3 Ma (Li et al., 2014; Liu et al., 2014b), both using zircon U-Pb geochronology. These age results reveal a relatively protracted history of intrusive activity in the deposit area of ~7 m.y..

Three molybdenite Re-Os isochron ages (ICP-MS) have been reported for the Mo mineralization at Chalukou. They are 150.0 ± 2.0, 148.0 ± 1.0 and 147.0 ± 1.0 Ma (Nie et al., 2011; Liu et al., 2014b; Zhang and Li, 2017). Zhang and Li (2017) proposed a robust mineralization age of 150.0 ± 2.0 Ma using the Re–Os isochron method, which is consistent with the age of the granite porphyry (152 ± 2 Ma, Zhang and Li, 2017). The Mo mineralization, obviously, is much shorter compared to the whole magmatism history (from 172 to 128 Ma, Zhang and Li, 2017). By contrast, Liu et al. (2017) proposed a more extended mineralization history of ~7 m.y. (from 152 to 145 Ma) because of a wide range of the Re-Os model ages as well as the intrusion ages. The age of the mineralization is thus still unresolved as is its duration. Moreover, all the molybdenite samples analyzed by these studies and Nie et al. (2011) were collected from the deepest part of the deposit (>700 m; e.g., from 761 to 1024 m, Liu et al., 2014b; from 737 to 1283 m, Zhang and Li, 2017), and were hosted by the fine-grained porphyry and its volcanic host.

In a deposit that may have a protracted mineralization history, it is inappropriate to construct an isochron from samples obtained from different vein-types, such as it was done in previous studies (Nie et al., 2011; Liu et al., 2014b; Liu et al., 2017). Moreover, we note that the analytical method (ICP-MS) used in previous studies (Liu et al., 2017) may have limited their ability to resolve multiple mineralization events due to its lower precision compared to the ID-N-TIMS method used in this study. They also did not establish the relative chronology of the molybdenite-quartz veins that were dated (Nie et al., 2011; Liu et al., 2014b; Zhang and Li, 2017). The previously reported molybdenite Re-Os model ages for the Chalukou deposit range between 150 ± 2 and 145 ± 2 Ma, implying that molybdenite mineralization occurred in a protracted timeframe (Nie et al., 2011; Liu et al., 2014b; Liu et al., 2017; Zhang and Li, 2017). In the present study, we reconstruct the temporal evolution of the Chalukou hydrothermal system by establishing the relative timing of the different vein types from cross-cutting relationships and determining their absolute ages using high-precision ID-N-TIMS Re-Os radiometric analyses. We also evaluate the temporal relationships of the veins to their spatially-associated intrusions. By doing so, we are able to rigorously address the question of whether or not the Chalukou deposit was the product of a single protracted mineralizing event involving multiple intrusions.

Hydrothermal alteration

Five types of alteration, potassic, silicic, sericitic, argillic and propylitic, affected the rocks of the Chalukou deposit (Fig. 3B). On surface, the altered rocks cover an area of ~ 3 km^2, but this increases to more than 8 km^2 at a depth of 600 m. The Mo mineralization is closely associated spatially with potassic and sericitic alteration of the granite porphyry and fine-grained porphyry.

Potassic alteration, manifested mainly as the replacement of plagioclase by K-feldspar, was developed in two zones, one of which was related to emplacement of the granite porphyry (~400 m depth) and the other to the fine-grained porphyry (>600 m depth) (Fig. 3B). Both zones of potassic alteration are developed in these intrusions as well as the Lower Ordovician volcanic rocks and both are associated with high grade Mo mineralization. Moreover, in both zones, the alteration is most intense where the granite porphyry and fine-grained porphyry are in contact with the volcanic rocks (Fig. 3B). Potassically altered rocks are characterized by the assemblage K-feldspar - quartz - molybdenite ± minor biotite ± magnetite ± anhydrite ± fluorite. Silicic alteration is restricted to the

234 apex of the fine-grained porphyry. In contrast, sericitic and argillic alterations are widespread. Rocks
235 subjected to sericitic alteration contain the fine-grained assemblage muscovite - quartz -
236 molybdenite ± pyrite ± minor fluorite, whereas argillic alteration was identified by the assemblage
237 quartz - illite - calcite ± pyrite ± minor galena ± sphalerite ± chalcopyrite. These alteration facies
238 resulted from the emplacement of the fine-grained porphyry and both overprint potassic alteration.
239 Propylitic alteration (epidote - chlorite ± calcite) is mainly observed in the Neoproterozoic
240 metamorphic rocks and Lower Ordovician volcanic rocks (Fig. 3B).

241 **Vein Classification**

242 On the basis of crosscutting relationships and mineralogy, two separate stages of Mo
243 mineralization and more than 10 distinct vein types have been recognized in the Chalukou deposit
244 (Table 1). There was an early stage of minor Mo mineralization related to the emplacement of the
245 granite porphyry and a later main stage of Mo mineralization associated with the emplacement of
246 the fine-grained porphyry (see below). These two stages were both succeeded by Pb-Zn
247 mineralization (see also Jin et al., 2014 and Li et al., 2019).

248 In describing the veins, we have used the nomenclature of Gustafson and Hunt (1975) and Sillitoe
249 (2010) in which the A veins are quartz veins with minor to no sulfide content, the B veins are quartz
250 veins with potassic alteration haloes that host the molybdenite mineralization, and the D veins refer
251 to quartz-pyrite veins with sericite selvages. In the following descriptions, the numbers 1 and 2
252 indicate the relative timing of different generations of the same vein-type and the letters E and M
253 are used as subscripts to identify veins associated with the early and main stage mineralization,
254 respectively.

255 The earliest veins are barren $A1_E$ quartz veins hosted by granite porphyry at shallow depth (<400
256 m) and are < 5 mm wide (Fig. 4A, B). The $B1_E$ veins are also hosted by granite porphyry, contain
257 the assemblage quartz + molybdenite + pyrite, and are surrounded by potassic alteration haloes.
258 Molybdenite is usually concentrated at the margins of the veins. The $B1_E$ veins crosscut the $A1_E$
259 veins (Fig. 4A), confirming that they formed later than the $A1_E$ veins. (Fig. 4A). They are crosscut
260 by $A2_E$ veins (Fig. 4C), which contain K-feldspar, quartz and disseminated molybdenite. The
261 youngest veins hosted by granite porphyry are molybdenite-dominant $B2_E$ veins that contain minor
262 proportions of quartz. In contrast to the B1 veins, they have sericitic alteration haloes (Fig. 4D).

Both the $A1_E$ and $A2_E$ veins are truncated by $B2_E$ veins, however, crosscutting relationships between $B1_E$ and $B2_E$ veins were not observed.

The barren A_M veins are hosted by fine-grained porphyry, which have the assemblage quartz + minor fluorite + minor pyrite. The A_M veins are surrounded by potassic alteration envelopes (Figs. 4E, 5A), and cut numerous USTs in the apex of the fine-grained porphyry (Fig. 4E), which are interpreted to represent a magmatic-hydrothermal transition. These A veins are thicker than the A_E veins, ranging in width from 3 to 10 mm. The $B1_M$ and $B2_M$ veins are hosted mainly by the fine-grained porphyry and also by the volcanic rocks. They contain the assemblage quartz + K-feldspar + molybdenite + minor pyrite (Fig. 5), and are the main Mo-bearing veins in the ore deposit (Jin et al., 2014). The molybdenite is usually concentrated along the margins of the $B1_M$ (Fig. 5A) or in sutures at their centers (Fig. 5B), whereas the $B2_M$ veins are extremely thin (< 2 mm) and Mo-dominant (Fig. 5C, D). Some $B2_M$ veins that contain breccia fragments of granite porphyry and the early-formed quartz-molybdenite veins cut the A_M veins (Fig. 4I). The late D_M veins contain pyrite ± quartz ± fluorite and minor chalcopyrite, molybdenite, sphalerite and galena and have well-developed sericitic alteration haloes. These veins crosscut all the other veins described above (Fig. 4G, H) and therefore post-dated the main stage of Mo mineralization. Rare quartz + magnetite/hematite veins (Fig. 4F) are observed at depth in the deposit (>1000 m), but their relationship with the other vein types is unclear.

Sampling and analytical methods

Zircon LA-ICP-MS U-Pb dating

Samples of granite porphyry, quartz porphyry, fine-grained porphyry and diorite porphyry were collected from underground workings and drill core of the eastern exploration zone for zircon LA-ICP-MS U-Pb dating. Zircon separation and cathodoluminescence (CL) imaging were carried out by the Hongxin Geological Exploration Technology Service Co., Ltd., Langfang, China. The samples were crushed and broken to a grain-size of ~100 μm. Zircon grains were separated using magnetic and heavy liquid separation methods and crystals were finally selected with the aid of a binocular microscope. These crystals and the Qinghu zircon standard were set in an epoxy resin disk and polished for analysis. The CL imaging of the polished zircon crystals was conducted on a JEOL scanning electron microscope and was done to examine zircon textures.

Zircon U-Pb dating was carried out in the State Key Laboratory of Geological Processes and Mineral Resources, China University of Geosciences Beijing (CUGB). The crystals were ablated using an excimer laser ablation system and an Agilent 7500a ICP-MS. The spot size was 30 μm and the laser repetition rate was 10 Hz. During laser ablation, a mixture of helium and argon was used as a carrier gas to enhance the transport efficiency of the ablated materials. The calibration of U, Th and Pb concentrations was carried out using ^{29}Si and NIST 610 glass as internal and reference standards, respectively. Zircon 91500 was adopted as the external standard (Wiedenbeck et al., 1995) to normalize isotopic fractionation and instrumental mass bias during analysis. Uranium-Pb isotope data were calculated and plotted using Isoplot 3.0 (Ludwig, 2003).

Molybdenite Re-Os dating

Molybdenite hosted by the different vein-types at various depths in the potassic and sericitic alteration zones was carefully selected, crushed (without direct metal contact), and handpicked under a binocular microscope (Fig. 7). Any residual material from the silicate matrix, e.g., quartz, was removed by loading the sample into a Savillex Teflon digestion vessel with 10 ml 32N HF and leaving it at room temperature for 24 h (Lawley and Selby, 2012). This process was repeated until most of the residual quartz had been digested. The molybdenite samples were then rinsed three times with Milli-Q water (MQ) and further rinsed in ethanol to remove any remaining HF. The cleaned samples were dried at 30 °C and further purified using a heavy liquid and handpicked under a binocular microscope. After a final stage of cleaning in an ultrasonic bath, the mineral separate comprised >95% molybdenite.

Molybdenite Re-Os isotopic analysis was carried out at the Laboratory for Sulfide and Source Rock Geochronology and Geochemistry at Durham University, United Kingdom, a member of the Durham Geochemistry Centre. The Re-Os analytical protocol followed that recommended by Selby and Creaser (2001) and Li et al. (2017b). A weighed aliquot of molybdenite and spike solution (^{185}Re plus isotopically normal Os) was loaded into a Carius tube with 11 N HCl (3 ml) and 15.5 N HNO_3 (6 ml), sealed and placed in a Carius tube, and digested at 220 °C in an oven for ~24 h. Osmium was purified from the acid medium using solvent extraction ($CHCl_3$) at room temperature and micro-distillation methods. The rhenium fraction was isolated by sodium hydroxide-acetone solvent extraction and HCl-HNO_3 anion chromatography. The purified rhenium and osmium were loaded

321 onto Ni and Pt filaments, respectively, and their isotopic compositions were measured using isotope
322 dilution-negative-thermal ionization mass spectrometry (ID-N-TIMS, Creaser et al., 1991).
323 The isotopic analysis was conducted on a Thermo Scientific TRITON mass spectrometer in the
324 Arthur Homes Laboratory at Durham University, with Re and Os isotopic compositions measured
325 using the static Faraday collection mode. The uncertainties in the Re and Os concentrations and Re-
326 Os isotope ratios were determined by propagating the spike calibration, the sample and spike weight
327 uncertainty, the reproducibility of Re and Os isotope standard values, as well as the blank
328 abundances and isotopic compositions that were run alongside the molybdenite analysis. A full
329 analytical protocol blank measured alongside the molybdenite analyses was 2.4 pg for Re and 0.1
330 pg for Os, with a $^{187}Os/^{188}Os$ ratio of 0.21 ± 0.02. Molybdenite Re-Os model ages were calculated
331 using the equation $t = \ln (^{187}Os/^{187}Re + 1)/\lambda$, employing a λ value of $1.666\times10^{-11} \pm 5.165\times10^{-14}$ a^{-1}
332 (Smoliar et al., 1996; Selby et al., 2007). The uncertainties of the Re-Os model age are presented
333 as ± x/y/z (analytical uncertainty /+tracer calibration /+decay constant uncertainties). To
334 evaluate the accuracy and reproducibility of the molybdenite Re-Os analytical approach, we also
335 analyzed the NIST molybdenite reference material (RM 8599). This analysis returned an age (27.65
336 ± 0.19 Ma) in agreement with the recommended age (27.656 ± 0.022 Ma, Markey et al., 2007;
337 Zimmerman et al., 2014) and ages previously determined in the Durham laboratory (e.g., Lawley
338 and Selby, 2012; Li et al., 2017b; Chang et al., 2017).

339 **Results**

340 **Zircon U-Pb ages**

341 Zircon crystals from all the samples are euhedral, colorless and transparent, and range from 50 to
342 250 μm in length with length/width ratios between 1:1 and 4:1. The CL images show that most of
343 the crystals have planar or oscillatory concentric zoning and some crystals contain inherited zircon.
344 The results of the zircon U-Pb age determinations for the different rock samples from the Chalukou
345 deposit are shown in Figure 6 and reported in Table 2. Inherited zircon with domains returning older
346 $^{206}Pb/^{238}U$ ages than the rest of crystal was not considered in determining the age of the sample.
347 Zircon crystals from the granite porphyry (CLK157) have U and Th concentrations of 355 to 844
348 and 213 to 643 ppm, respectively, and Th/U ratios from 0.44 to 1.16. Nineteen concordant analyses
349 yielded a weighted mean $^{206}Pb/^{238}U$ age of 148.8 ± 1.1 Ma (MSWD= 1.4; Fig. 6A). The quartz

porphyry (CLK164) has zircon crystals containing between 59 and 749 ppm U and 51 and 943 ppm Th. Their Th/U ratios range from 0.54 to 2.61. Eleven zircon crystals produced a concordant weighted mean $^{206}Pb/^{238}U$ age of 147.5 ± 2.1 Ma (MSWD= 0.4; Fig. 6B). Zircon crystals from the fine-grained porphyry (CLK69) contain 57 to 132 ppm U and 54 to 211 ppm Th, and have Th/U ratios from 0.84 to 1.60. These crystals (eight) yielded a weighted mean $^{206}Pb/^{238}U$ age of 147.4 ± 2.7 Ma (MSWD = 0.4; Fig. 6C). Finally, zircon crystals from the diorite porphyry (CLK176) have U and Th contents ranging from 33 to 403 and 45 to 239 ppm, respectively, and a Th/U ratio varying from 0.37 to 1.56. Nine zircon grains yielded a weighted mean $^{206}Pb/^{238}U$ age of 138.9 ± 2.3 Ma (MSWD = 1.7; Fig. 6D).

Molybdenite Re-Os ages

Two samples of A veins and four samples of B veins containing 4.2 to 45.2 ppm Re were selected for high-precision molybdenite ID-N-TIMS Re-Os age determination. The results are provided in Table 3 and are listed with three different sets of errors. The first error contains only analytical uncertainty which is used to compare Re-Os ages produced in this study. The second error contains analytical and spike uncertainties which allow our data to be compared to Re-Os dates produced in other laboratories. The third error adds the additional uncertainty of the decay constant to allow for comparisons to other isotopic systems (e.g., U-Pb). Molybdenite from a $B1_E$ vein sample (Fig. 7A), representative of the early Mo mineralization, returned a Re-Os model age of 153.96 ± 0.08/0.63/0.79 Ma, which is significantly older than previously determined Re-Os ages for the Chalukou deposit (147-148 Ma; Nie et al., 2011; Liu et al., 2014b). Within uncertainty, this age is the same as a zircon U-Pb age of 154 ± 1 Ma for the granite porphyry reported by Duan et al. (2018). Later $A2_E$ and $B2_E$ veins from the early mineralizing stage yielded Re-Os dates of 150.28 ± 0.06/0.62/0.78 and 148.67 ± 0.07/0.62/0.77 Ma, respectively (Fig. 7B, C). Molybdenite in A_M and two $B2_M$ veins from the main Mo mineralization stage (Fig. 7D, E and F) yielded model ages of 147.49 ± 0.09/0.60/0.76, 147.67 ± 0.10/0.60/0.76, and 147.04 ± 0.12/0.72/0.86 Ma, respectively, which are identical to the Re-Os age referred to above reported by Nie et al. (2011) and Liu et al. (2014b), though the analytical precision of our data is considerably better (Fig. 8A).

Discussion

Multiple veins formation

Although several geochronological studies have been conducted on the Chalukou porphyry Mo deposit, the limited characterization of dated samples and the limited precision from previous measurements makes any determination of the exact duration of mineralization at Chalukou difficult (Fig. 8A; Nie et al., 2011; Li et al., 2014; Liu et al., 2014b; Zhang and Li, 2017; Duan et al., 2018). Nie et al. (2011) and Liu et al., (2014b) interpreted the age of 147 ± 1 and 148 ± 1 Ma to indicate that the Chalukou deposit formed in the late Jurassic. However, the association of separate sets of A and B veins with the granite porphyry (148.8 ± 1.1 Ma) and the fine-grained porphyry (147.4 ± 2.7 Ma) and the crosscutting relationships among these vein types in each association (Fig. 4B, C) are evidence that the Chalukou deposit probably was the product of more than one magmatic-hydrothermal pulse. Zircon U-Pb ages of intrusions in the Chalukou mine area, also show that the history of magmatic activity potentially associated with mineralization was much longer (154-147 Ma; Zhang and Li, 2017). Subsequently, Liu et al. (2017) reinterpreted the Re-Os ages for molybdenite obtained by Nie et al. (2011) and Liu et al. (2014b) to indicate that the mineralization was introduced over a period of 5 m.y., and thus proposed that the Chalukou deposit was the result of a long-lived ore-forming system in which multiphase igneous activity played a crucial role. Moreover, the early-formed quartz-molybdenite veins were brecciated and cemented by subsequent quartz and molybdenite (Fig. 4I). The quartz-molybdenite breccias have very similar mineral assemblages and textures to the $B1_M$ veins that crosscut the A_M veins (Fig. 4I), indicating that the breccias formed later than $B1_M$ veins and probably were coeval with the $B2_M$ veins.

Magmatism and Mo mineralization

The oldest Re-Os age determined in this study is from a $B1_E$ vein (153.96 ± 0.08/0.63/0.79 Ma, Table 3) and is interpreted to represent the age of the early Mo mineralization (Fig. 8B). This vein, which has a potassic alteration halo, is hosted by the granite porphyry. In principle, the early mineralization could have been the product of fluids from the monzogranite, or the ore-hosted granite porphyry. We propose that the early Mo mineralization is genetically associated with the granite porphyry (Fig. 3A) instead of the monzogranite for the following reasons: (1) the monzogranite is altered and mineralized only near its contacts with the fine-grained porphyry (Fig. 3B), and (2) the youngest zircon U-Pb age for the monzogranite is 162 ± 2 Ma (Liu et al., 2014b), making it at least 8 m.y. older than the oldest B vein (Fig. 8A). Thus, monzogranite is a pre-ore

intrusion and was not related to Mo mineralization. The Re-Os age of 153.96 ± 0.79 Ma is, within the analytical uncertainty, identical to a U-Pb age of 154 ± 1 Ma for the granite porphyry reported by Duan et al. (2018) and similar to an age for this intrusion (152 ± 2 Ma) reported by Zhang and Li (2017). This indicates that the early Mo deposition was synchronous with the emplacement of granite porphyry. The other two molybdenite samples ($A2_E$ and $B2_E$ veins) hosted by granite porphyry yielded Re-Os model ages of 150.28 ± 0.06/0.62/0.78 and 148.67 ± 0.07/0.62/0.77 Ma, respectively, which are consistent with our age of the granite porphyry (148.8 ± 1.1 Ma). These high-precision Re-Os ages therefore indicate that the early mineralization stage took place over a period of 5.29 ± 0.11 m.y. (Fig. 8C). This prolonged duration of the early Mo mineralization stage likely indicates more than one episode of hydrothermal activity and, given that the ages reported for the granite porphyry (154 ± 1 to 148 ± 1 Ma; Fig. 8A) cover this range, it is attractive to propose that granite porphyry intrusion was equally prolonged and is reasonable with known lifetimes of granite intrusions (Zhang and Li, 2017; Duan et al., 2018). Zircon U-Pb ages of the Cu-bearing tonalite intrusion (from 218.9 ± 3.1 to 205.8 ± 2.1 Ma; Kobylinski et al., 2020) also indicated a long magmatic and mineralization history at the Gibraltar Cu-Mo deposit, Canada. Without detailed information on the locations of the samples analyzed in previous studies, we cannot, however, rule out the possibility that the range of ages reported for the granite porphyry is an artefact of analysis resulting from differences in the methods employed by different groups at different laboratories.

The main stage Mo orebodies are hosted by the fine-grained porphyry and its adjacent volcanic rocks (Fig. 3B). Molybdenite in an A_M vein and two $B2_M$ veins yielded Re-Os model ages from 147.67 ± 0.10/0.60/0.76 to 147.04 ± 0.12/0.72/0.86 Ma (Table 3 and Fig. 8B), which are identical to the age of the fine-grained porphyry (147.4 ± 2.7 Ma). All the molybdenite Re-Os ages reported in this study for the main Mo mineralization stage veins spatially associated with the fine-grained porphyry are consistently younger than those associated with granite porphyry. The small absolute uncertainty in our Re-Os ages enables us to separate temporally the molybdenite hosted by the shallowly emplaced granite porphyry from that related to the more deeply-seated fine-grained porphyry. These data indicate that there were at least two magmatic-hydrothermal events during the formation of the Chalukou Mo deposit, occurring at 153.96 ± 0.08 and 148.67 ± 0.07 Ma, with the majority of the Mo resource produced by magmatic-hydrothermal fluids released from the fine-grained porphyry at 147 Ma during an interval of <650 Ka (Fig. 8C).

438 **Implications for giant porphyry Mo systems**

439 The time taken to form a giant porphyry type deposit and whether it forms during a single event
440 or multiple events have long been debated (Mathur et al., 2000; Selby and Creaser, 2001; von Quadt
441 et al., 2011; Braxton et al., 2012; Deckart et al., 2012, 2014; Chiaradia et al., 2013; Stein, 2014;
442 Spencer et al., 2015; Buret et al., 2016). Geochronological studies have reported evidence for
443 multiple pulses of mineralization for magmatic-hydrothermal systems of both long (several m.y.,
444 e.g., Los Pelambres-El Pachón, Deckart et al., 2014; El Teniente, Spencer et al., 2015; Yulong,
445 Chang et al., 2017, 2018), and short duration (tens to hundreds of k.y., e.g., Qulong, Li et al., 2017a,
446 b). The two giant porphyry Cu(-Mo) deposits in Tibet, SW China, namely Qulong and Yulong, are
447 the largest and the third largest porphyry Cu deposits in China, respectively (Yang and Cooke, 2019).
448 Both of them are considered to have formed from multiple mineralization pulses, however, the
449 Qulong deposit, which has the larger Cu resource, is interpreted to have formed in 266 ± 13 k.y.,
450 whereas the Yulong deposit formed over a duration of 5.13 ± 0.23 m.y. (Chang et al., 2017; Li et al.,
451 2017b). Therefore, the duration of mineralization may not be an important factor in the formation
452 of a giant porphyry deposit (Fig. 9A).

453 Many porphyry Cu deposits have experienced a relatively long intrusive history (~3 m.y., Wallace,
454 1995; Maksaev et al., 2004; Masterman et al., 2005; Harris et al., 2008; Kobylinski et al., 2020) and
455 duration of mineralization. This is also true for porphyry Mo deposits (e.g., Endako, ~3 m.y.,
456 Anderson et al., 1998; Henderson, ~2 m.y., Seedorff and Einaudi, 2004; Climax, ~9 m.y., Bookstrom,
457 1989; Wallace, 1995; Yuchiling, ~7 m.y., Li et al., 2013; Fig. 9A). It should be noted, however, that
458 the mineralization ages obtained from Mesozoic porphyry Mo deposits have much greater
459 uncertainty associated with them than those from Cenozoic deposits (Fig. 9B), which tends to
460 increase estimates of the duration of the Mesozoic ore systems.

461 The overall longevity of the Chalukou deposit (6.92 ± 0.15 m.y.) implies at least two separate
462 magmatic-hydrothermal events as described above. It should be noted that, however, most of the
463 Mo ores (more than 90% to the bulk ore reserves) related to the emplacement of the fine-grained
464 porphyry at the Chalukou giant Mo deposit were formed at ~147 Ma within a duration of 0.63 ±
465 0.16 Ma. Although recent detailed Re-Os dating of molybdenite has provided evidence of multiple
466 mineralization pulses during the formation of some giant porphyry deposits (e.g., Deckart et al.,
467 2014; Spencer et al., 2015; Li et al., 2017b), their contributions to the overall metal budget in

individual ore deposits vary considerably (Chang et al., 2017). As was the case for Mo at Chalukou, most of the Cu (> 80%) in the Yulong porphyry Cu deposit was introduced in a short period of time (0.82 ± 0.24 m.y.) in a longer cycle magmatic-hydrothermal activity (5.13 ± 0.23 m.y., Chang et al., 2017). The Cu mineralization at Bajo de la Alumbrera was even more rapid (0.029 m.y., Buret et al., 2016) but, as at Chalukou and Yulong, was the product of a much longer-lived episode of magmatism. Finally, we note that at the El Teniente Cu-Mo porphyry deposit Mo and Cu were introduced separately; the Cu mineralization occurred between 6.3 and 4.6 Ma, whereas the bulk of the Mo was introduced between 4.80 and 4.58 Ma (Spencer et al., 2015). Spencer et al. (2015) concluded that within these time intervals for Cu and Mo there were multiple mineralization events of roughly 100 Ka separated by barren events of much longer duration. The overarching conclusion of these studies is that the bulk of the mineralization in porphyry systems typically takes place in one or more events of relatively short duration separated by barren intervals time of highly variable length.

More than 37 billion metric tons (Gt) of fluid would have been required to precipitate the main stage mineralization in the Chalukou deposit (90% of the total 2.46 Mt Mo resource), assuming a constant Mo concentration in the fluid (e.g., 60 ppm maximum, Audétat, 2015; Shang et al., 2020). Given the duration of 650 Ka estimated for this hydrothermal system, this corresponds to a flux of 1.8 kg/s. The estimated flux of Chalukou is comparable to the estimated flux of 6.0 kg/s for the El Teniente Mo mineralization (2.5 Mt over 220 Ka; Spencer et al., 2015). An important mechanism thought to be important for formation of porphyry type deposits is the expulsion of a large amount of fluids that may be stored at the top of the magma chamber, providing the necessary flux of fluids required to form these deposits (Ulrich et al., 2002; Sillitoe, 2010; Buret et al., 2016). We cannot distinguish if there are pulses shorter than few tens of k.y. based on the precision of our measurements (Cathles et al, 1997; Weis et al., 2012; Mercer et al., 2015). However, based on the geological and geochronological evidences for Chalukou of this study, we think that a strong case can be made that the main stage mineralization was introduced by a single fine-grained porphyry intrusion and that the main stage mineralization was a restricted temporal event of < 650 Ka.

Conclusions

High-precision molybdenite Re-Os age determinations reveal that there were two magmatic-

hydrothermal events at Chalukou, an early event between 153.96 ± 0.08/0.63/0.79 and 148.67 ± 0.07/0.62/0.77 Ma, and a much shorter event between 147.67 ± 0.10/0.60/0.76 and 147.04 ± 0.12/0.72/0.86 Ma that produced the bulk of the deposit. The early event was associated with the emplacement of several intrusions of granite porphyry, whereas the main Mo mineralizing event, which produced over 90% of the resource, was coincident with the intrusion of a single body of fine-grained porphyry. Most of the molybdenite was deposited in the $B1_M$ and $B2_M$ veins that accompanied potassic alteration in the deeper part of the system (>600 m) by fluids that are interpreted to have originated from the fine-grained porphyry. The new high-precision ID-N-TIMS Re-Os age results reported in this contribution indicate that, although multiple hydrothermal events may have been essential for the formation of some giant porphyry Cu and Cu-Mo deposits, the giant Chalukou porphyry Mo deposit, the only porphyry Mo deposit, for which this issue has been addressed, was effectively the product of a single short-lived episode (<650 Ka) of magmatic-hydrothermal activity.

Acknowledgments

This research was supported financially by the National Natural Science Foundation of China (Grants 41503042, 41973038), the Fundamental Research Funds for the Central Universities (Grants QZ05201904, 2652018169), the MOST Special Fund from the State Key Laboratory of Geological Processes and Mineral Resources, China University of Geosciences (Grant MSFGPMR201804), and the 111 Project of the Ministry of Science and Technology (BP0719021). DS thanks Antonia Hoffman, Geoff Nowell and Chris Ottley for technical support. DS acknowledges the Total Endowment Fund and the CUG (Wuhan) Dida scholarship. We thank Li Su and Hongyu Zhang (CUGB) for performing the U-Pb analyses. Constructive suggestions from an anonymous reviewer, Associate Editor Massimo Chiaradia, and Editor-in-Chief Larry Meinert significantly improved this manuscript. DZ was supported financially by the China Scholarship Council (CSC) (201906405012) for a visit to McGill University.

References

Anderson, R.G., Whalen, J.B., and Villeneuve, M.E., 1998, Mesozoic to Tertiary volcanism and plutonism in southern Nechako NATMAP area. Part 2: Triassic to Eocene composite intrusions and molybdenum metallogeny: The Endako batholith redefined: New geological constraints on

Mesozoic to Tertiary metallogenesis and mineral exploration in central British Columbia, in Struik, L.C., and MacIntyre, D.G., eds., Nechako NATMAP Project, Geological Association of Canada, Cordilleran Section, Short Course Notes, March 27, 1998, 27 p.

Audétat, A., 2015, Compositional evolution and formation conditions of magmas and fluids related to porphyry Mo mineralization at Climax, Colorado: Journal of Petrology, v. 56, p. 1519–1546.

Barra, F., Ruiz, J., Mathur, R., and Titley, S., 2003, A Re-Os study on sulfide minerals from the Bagdad porphyry Cu-Mo deposit, northern Arizona, United States: Mineralium Deposita, v. 38, p. 585–596.

Bookstrom, A. A., 1989, The Climax–Alma granite batholith of Oligocene age and the porphyry molybdenum deposits of Climax, Colorado, U.S.A: Engineering Geology, v. 27, p. 543–568.

Braxton, D.P., Cooke, D.R., Dunlap, J., Norman, M., Reiners, P., Stein, H., and Waters, P., 2012, From crucible to graben in 2.3 Ma: A high-resolution geochronological study of porphyry life cycles, Boyongan-Bayugo coppergold deposits, Philippines: Geology, v. 40, p. 471–474.

Buret, Y., von Quadt, A., Heinrich, C., Selby, D., Wälle, M., and Peytcheva, I., 2016, From a long-lived upper-crustal magma chamber to rapid porphyry copper emplacement: Reading the geochemistry of zircon crystals at Bajo de la Alumbrera (NW Argentina): Earth and Planetary Science Letters, v. 450, p. 120–131.

Carten, R.B., Geraghty, E.P., Walker, B.M., and Shannon, J.R., 1988, Cyclic development of igneous features and their relationship to high-temperature hydrothermal features in the Henderson porphyry molybdenum deposit, Colorado: Economic Geology, v. 83, p. 266–296.

Cathles, L.M., Erendi, A.H.J., and Barrie, T., 1997, How long can a hydrothermal system be sustained by a single intrusive event?: Economic Geology, v. 92, p. 766–771.

Chang, J., Li, J.W., Selby, D., Liu, J.C., and Deng, X.D., 2017, Geological and chronological constraints on the long-lived Eocene Yulong porphyry Cu-Mo deposit, eastern Tibet: Implications for the lifespan of giant porphyry Cu deposits: Economic Geology, v. 112, p. 1719–1746.

Chang, J., Li, J.W., and Audétat, A., 2018, Formation and evolution of multistage magmatic-hydrothermal fluids at the Yulong porphyry Cu-Mo deposit, eastern Tibet: Insights from LA-ICP-MS analysis of fluid inclusions: Geochimica et Cosmochimica Acta, v. 232, p. 181–205.

Chen, Y.J., Zhang, C., Li, N., Yang, Y.F., and Deng, K., 2012, Geology of the Mo deposits in Northeast China: Journal of Jilin University (Earth Science Edition), v. 42, p. 1224–1268 (in Chinese with English abstract).

Chen, Y.J., Zhang, C., Wang, P., Pirajno, F., and Li, N., 2017, The Mo deposits of Northeast China: A powerful indicator of tectonic settings and associated evolutionary trends: Ore Geology Reviews,

v. 81, p. 602–640.

Chiaradia, M., Merino, D., and Spikings, R., 2009a, Rapid transition to long-lived deep crustal magmatic maturation and the formation of giant porphyry-related mineralization (Yanacocha, Peru): Earth and Planetary Science Letters, v. 288, p. 505–515.

Chiaradia, M., Vallance, J., Fontboté, L., Stein, H., Schaltegger, U., Coder, J., Richards, J., Villeneuve, M., and Gendall, I., 2009b, U-Pb, Re-Os, and $^{40}Ar/^{39}Ar$ geochronology of the Nambija Au skarn and Pangui porphyry Cu deposits, Ecuador: Implications for the Jurassic metallogenic belt of the Northern Andes: Mineralium Deposita, v. 44, p. 371–387.

Chiaradia, M., Schaltegger, U., Spikings, R., Wotzlaw, J-F., and Ovtcharova, M., 2013, How accurately can we date the duration of magmatic-hydrothermal events in porphyry systems?—an invited paper: Economic Geology, v. 108, p. 565–584.

Chiaradia, M., Schaltegger, U., and Spikings, R.A., 2014, Time scales of mineral systems—advances in understanding over the past decade: Society of Economic Geologists, Special Publication 18, p. 37–58.

Cooke, D.R., Hollings, P., and Walshe, J.L., 2005, Giant porphyry deposits: Characteristics, distribution, and tectonic controls: Economic Geology, v. 100, p. 801–818.

Creaser, R.A., Papanastassiou, D.A., and Wasserburg, G.J., 1991, Negative thermal ion mass spectrometry of osmium, rhenium and iridium: Geochimica et Cosmochimica Acta, v. 55, p. 397–401.

Dai, J.Z., Mao, J.W., Yang, F.Q., Ye, H.S., Zhao, C.S., Xie, G.Q., and Zhang, C.Q., 2006, Geological characteristics and geodynamic background of molybdenum (copper) deposits along Yanshan-Liaoning metallogenic belt on northern margin of North China block: Mineral Deposits, v. 25, p. 598–615 (in Chinese with English abstract).

Dai, J.Z., Mao, J.W., Zhao, C.S., Xie, G.Q., Yang, F.Q., and Wang, Y.T., 2009, New U-Pb and Re-Os age data and the geodynamic setting of the Xiaojiayingzi Mo (Fe) deposit, Western Liaoning province, Northeastern China: Ore Geology Reviews, v. 35, p. 235–244.

Deckart, K., Clark, A.H., Cuadra, P., and Fanning, M., 2012, Refinement of the time-space evolution of the giant Mio-Pliocene Río Blanco-Los Bronces porphyry Cu-Mo cluster, Central Chile: New U-Pb (SHRIMP II) and Re-Os geochronology and $^{40}Ar/^{39}Ar$ thermochronology data: Mineralium Deposita, v. 48, p. 57–79.

Deckart, K., Silva, W., Spröhnle, C., and Vela, I., 2014, Timing and duration of hydrothermal activity at the Los Bronces porphyry cluster: an update: Mineralium Deposita, v. 49, p. 535–546.

Dilles, J.A., Martin, M.W., Stein, H., and Rusk, B., 2003, Re-Os and U-Pb ages for the Butte copper

district, Montana: A short- or long-lived hydrothermal system?: Geological Society of America Abstract with Programs, v. 35, p. 400.

Duan, P.X., Liu, C., Mo, X.X., Deng, D.F., Qin, J.H., Zhang, Y., and Tian, S.P., 2018, Discriminating characters of ore-forming intrusions in the super-large Chalukou porphyry Mo deposit, NE China: Geoscience Frontiers, v. 9, p.1417–1431.

Fu, R.Z., Kan, X.S., Meng, Z.J., and Wang, J.P., 2011, Geological characteristics of Chalukou porphyry molybdenum polymetallic deposit Daxinganling, Heilongjiang Province: Mineral Exploration, v. 2, p. 232–240 (in Chinese with English abstract).

Gao, B.Y., Zhang, L.C., Jin, X.D., Li, W.J., Chen, Z.G., and Zhu, M.T., 2016, Geochronology and geochemistry of the Badaguan porphyry Cu-Mo deposit in Derbugan metallogenic belt of the NE China, and their geological significances: International Journal of Earth Sciences, v. 105, p. 507–519.

Gustafson, L.B., and Hunt, J.P., 1975, The porphyry copper deposit at El Salvador, Chile: Economic Geology, v. 70, p. 857–912.

Harris, A.C., Dunlap, W.J., Reiners, P. W., Allen, C.M., Cooke, D.R., White, N.C., Campbell, I.H., and Golding, S.D., 2008, Multimillion year thermal history of a porphyry copper deposit: Application of U-Pb, $^{40}Ar/^{39}Ar$ and (U-Th)/He chronometers, Bajo de la Alumbrera copper-gold deposit, Argentina: Mineralium Deposita, v. 43, p. 295–314.

Hu, X.L., Ding, Z.J., He, M.C., Yao, S.Z., Zhu, B.P., Shen, J., and Chen, B., 2014, A porphyry-skarn metallogenic system in the Lesser Xing'an Range, NE China: Implications from U-Pb and Re-Os geochronology and Sr-Nd-Hf isotopes of the Luming Mo and Xulaojiugou Pb-Zn deposits: Journal of Asian Earth Sciences, v. 90, p. 88–100.

Jensen, P.W., 1998, A structural and geochemical study of the Sierrita porphyry copper system, Pima County, Arizona: Unpublished M.S. thesis, Tucson, University of Arizona, 136 p.

Jin, L.Y., Qin, K.Z., Meng, Z.J., Li, G.M., Song, G.X., Li, Z.Z., Lv, K.P., Kan, X.S., and Zhao, C., 2014, Vein features and occurrences in Chalukou giant molybdenum-zinc-lead deposit, northern Great Xing'an Range, and its indications for mineralization: Mineral Deposits, v. 33, p. 742–760 (in Chinese with English abstract).

Klemm, L.M., Pettke, T., and Heinrich C.A., 2008, Fluid and source magma evolution of the Questa porphyry Mo deposit, New Mexico, USA: Mineralium Deposita, v. 43, p. 533–552.

Kobylinski, C., Hattori, K., Smith, S., and Plouffe, A., 2020, Protracted magmatism and mineralized hydrothermal activity at the Gibraltar porphyry copper-molybdenum deposit, British Columbia: Economic Geology, v. 115, p. 1119–1136.

Lawley, C.J.M., and Selby, D., 2012, Re-Os geochronology of quartz-enclosed ultrafine molybdenite: Implications for ore geochronology: Economic Geology, v. 107, p. 1499–1505.

Li, N., Chen, Y.J., Pirajno, F., and Ni, Z.Y., 2013, Timing of the Yuchiling giant porphyry Mo system, and implications for ore genesis: Mineralium Deposita, v. 48, p. 505–524.

Li, Y., Li, X.H., Selby, D., and Li, J.W., 2017a, Pulsed magmatic fluid release for the formation of porphyry deposits: Tracing fluid evolution in absolute time from the Tibetan Qulong Cu-Mo deposit: Geology, v. 46, p. 7–10.

Li, Y., Selby, D., Condon, D., and Tapster, S., 2017b, Cyclic magmatic-hydrothermal evolution in porphyry systems: High-precision U-Pb and Re-Os geochronology constraints from the Tibetan Qulong porphyry Cu-Mo deposit: Economic Geology, v. 112, p. 1419–1440.

Li, Z.Z., Qin, K.Z., Li, G.M., Ishihara, S., Jin, L.Y., Song, G.X., and Meng, Z.J., 2014, Formation of the giant Chalukou porphyry Mo deposit in northern Great Xing'an Range, NE China: Partial melting of the juvenile lower crust in intra-plate extensional environment: Lithos, v. 202, p. 138–156.

Li, Z.Z., Qin, K.Z., Li, G.M., Jin, L.Y., and Song, G.X., 2019, Incursion of meteoric water triggers molybdenite precipitation in porphyry Mo deposits: A case study of the Chalukou giant Mo deposit: Ore Geology Reviews, v. 109, p. 144–162.

Liu, J., Mao, J.W., Wu, G., Wang, F., Luo, D.F., Hu, Y.Q., and Li, T.G., 2014a, Fluid inclusions and H-O-S-Pb isotope systematics of the Chalukou giant porphyry Mo deposit, Heilongjiang Province, China: Ore Geology Reviews, v. 59, p. 83–96.

Liu, J., Mao, J.W., Wu, G., Wang, F., Luo, D.F., and Hu, Y.Q., 2014b, Zircon U-Pb and molybdenite Re-Os dating of the Chalukou porphyry Mo deposit in the northern Great Xing'an Range, China, and its geological significance: Journal of Asian Earth Sciences, v. 79, p. 696–709.

——2015, Geochemical signature of the granitoids in the Chalukou giant porphyry Mo deposit in the Heilongjiang Province NE China: Ore Geology Reviews, v. 64, p. 35–52.

Liu, Y.F., Bagas, L., Jiang, S.H., and Wang, F.X., 2017, The Chalukou deposit in the North Great Xing'an Range of China: A protracted porphyry Mo ore-forming system in a long-lived magmatic evolution cycle: Ore Geology Reviews, v. 89, p. 171–186.

Long, K.R., 1995, Production and reserves of Cordilleran (Alaska to Chile) porphyry copper deposits: Arizona Geological Society Digest, v. 20, p. 35–69.

Ludwig, K.R., 2003, User's manual for Isoplot 3.00: A geochronological toolkit for Microsoft Excel: Berkeley, California, Berkeley Geochronology Center.

703 Maksaev, V., Munizaga, F., McWilliams, M., Fanning, M., Mathur, R., Ruiz, J., and Zentilli, M.,
704 2004, New chronology for El Teniente, Chilean Andes, from U-Pb, $^{40}Ar/^{39}Ar$, Re-Os and fission-
705 track dating: Implications for the evolution of a supergiant porphyry Cu-Mo deposit: Society of
706 Economic Geologists Special Publication 11, p. 15–54.
707
708 Markey, R., Stein, H.J., Hannah, J.L., Zimmerman, A., Selby, D., and Creaser, R.A., 2007,
709 Standardizing Re-Os geochronology: A new molybdenite reference material (Henderson, USA) and
710 the stoichiometry of Os salts: Chemical Geology, v. 244, p. 74–87.
711
712 Masterman, G.J., Cooke, D.R., Berry, R.F., Walshe, J.L., Lee, A.W., and Clark, A.H., 2005, Fluid
713 chemistry, structural setting, and emplacement history of the Rosario Cu-Mo porphyry and Cu-Ag-
714 Au epithermal veins, Collahuasi district, northern Chile: Economic Geology, v. 100, p. 835–862.
715
716 Mathur, R., Ruiz, J., Titley, S., Gibbins, S., and Margotomo, W., 2000, Different crustal sources for
717 Au-rich and Au-poor ores of the Grasberg Cu-Au porphyry deposit: Earth and Planetary Science
718 Letters, v. 183, p. 7–14.
719
720 Mercer, C.N., Reed, M.H., and Mercer, C.M., 2015, Time scales of porphyry Cu deposit formation:
721 Insights from titanium diffusion in quartz: Economic Geology, v. 110, p. 587–602.
722
723 Meng, Z.J., Kan, X.S., Li, X.C., Wang, J.P., Zhang, R.Z., Lu, K.P., Sun, Z.J., Shi, Y.J., Zhang, J.N.,
724 and Wang, H.Y., 2011, The discovery and exploration process of the Chalukou giant porphyry
725 molybdenum polymetallic deposit in forest-covered area of northeastern Da Higgnan Mountains
726 and its geological significance: Geology in China, v. 38, p. 1504–1517 (in Chinese with English
727 abstract).
728
729 Morelli, R.M., Bell, C.C., Creaser, R.A., and Simonetti, A., 2010, Constraints on the genesis of gold
730 mineralization at the Homestake gold deposit, Black Hills, South Dakota, from rhenium-osmium
731 sulfide geochronology: Mineralium Deposita, v. 45, p. 461–480.
732
733 Nie, F.J., Zhang,W.Y., Du, A.D., Jiang, S.H., and Liu, Y., 2007, Re-Os isotopic dating on
734 molybdenite separates from the Xiaodonggou porphyry Mo deposit, Hexigtenqi County, Inner
735 Mongolia: Acta Petrologica Sinica, v. 81, p. 898–905 (in Chinese with English abstract).
736
737 Nie, F.J., Sun, Z.J., Li, C., Liu, Y.F., Lv, K.P., Zhang, K., and Liu, Y., 2011, Re-Os isotopic dating
738 of molybdenite separates from Chalukou porphyry Mo polymetallic deposit in Heilongjiang
739 Province: Mineral Deposits, v. 30, p. 828–836 (in Chinese with English abstract).
740
741 Nie, F.J., Sun, Z.J., Liu, Y.F., Lv, K.P., Zhao, Y.A., and Cao, Y., 2013, Mesozoic multiple magmatic
742 activities and molybdenum mineralization in the Chalukou ore district, Da Hinggan Mountains:
743 Geology in China, v. 40, p. 273–386 (in Chinese with English abstract).
744
745 Qin, K.Z., Li, G.M., Zhao, J.X., Zhai, M.G., Zeng, Q.D., Gao, J., Xiao, W.J., Li, J.L., and Sun, S.,
746 2017, Links of Collage orogenesis of microcontinents and crust evolution to characteristic

metallogeneses in China: Acta Petrologica Sinica, v. 33, p. 305–325 (in Chinese with English Abstract).

Seedorff, E., and Einaudi, M.T., 2004, Henderson porphyry molybdenum system, Colorado: I. Sequence and abundance of hydrothermal mineral assemblages, flow paths of evolving fluids, and evolutionary style: Economic Geology, v. 99, p. 3−37.

Selby, D., and Creaser, R.A., 2001, Re-Os geochronology and systematics in molybdenite from the Endako porphyry molybdenum deposit, British Columbia, Canada: Economic Geology, v. 96, p. 197–204.

Selby, D., Creaser, R.A., Stein, H.J., Markey, R.J., and Hannah, J.L., 2007, Assessment of the ^{187}Re decay constant by cross calibration of Re-Os molybdenite and U-Pb zircon chronometers in magmatic ore systems: Geochimica et Cosmochimica Acta, v. 71, p. 1999–2013.

Shang, L.B., Williams-Jones, A.E., Wang, X.S., Timofeev, A., Hu, R.Z., and Bi, X.W., 2020, An experimental study of the solubility and speciation of MoO_3(s) in hydrothermal fluids at temperatures up to 350°C: Economic Geology, v. 115, p. 661–669.

Shu, Q.H, Chang, Z.S, Lai, Y., Zhou, Y.T, Sun, Y., and Yan, C., 2016, Regional metallogeny of Mo-bearing deposits in northeastern China, with new Re-Os dates of porphyry Mo deposits in the northern Xilamulun district: Economic Geology, v. 111, p. 1783–1798.

Sillitoe, R.H., 2010, Porphyry copper systems: Economic Geology, v. 105, p. 3–41.

Sillitoe, R.H., and Mortensen, J.K., 2010, Longevity of porphyry copper formation at Quellaveco, Peru: Economic Geology, v. 105, p. 1157–1162.

Smoliar, M.I., Walker, R.J., and Morgan, J.W., 1996, Re-Os ages of group IIA, IIIA, IVA, and IVB iron meteorites: Science, v. 271, p. 1099–1102.

Spencer, E.T., Wilkinson, J.J., Creaser, R.A., and Seguel, J., 2015, The distribution and timing of molybdenite mineralization at the El Teniente Cu-Mo porphyry deposit, Chile: Economic Geology, v. 110, p. 387–421.

Stein, H.J., Markey, R.J., Morgan, J.W., Hannah, J.L., and Schersten, A., 2001, The remarkable Re-Os chronometer in molybdenite: How and why it works: Terra Nova, v. 13, p. 479–486.

Stein, H., Scherstén, A., Hannah, J., and Markey, R., 2003, Subgrain-scale decoupling of Re and ^{187}Os and assessment of laser ablation ICP-MS spot dating in molybdenite: Geochimica et Cosmochimica Acta, v. 67, p. 3673–3686.

Stein, H.J., 2014, Dating and tracing the history of ore formation, in Turekian, H.D.H.K., ed., Treatise on Geochemistry (second edition): Oxford, UK, Elsevier, p. 87–118.

Ulrich, T., Gunther, D., and Heinrich, C.A., 2002, The evolution of a porphyry Cu-Au deposit, based on LA-ICP-MS analysis of fluid inclusions: Bajo de la Alumbrera, Argentina: Economic Geology, v. 97, p. 1889–1920.

von Quadt, A., Erni, M., Martinek, K., Moll, M., Peytcheva, I., and Heinrich, C.A., 2011, Zircon crystallization and the lifetimes of ore-forming magmatic-hydrothermal systems: Geology, v. 39, p. 731–734.

Wallace, S.R., 1995, SEG presidential address: the climax-type molybdenite deposits: what they are, where they are, and why they are: Economic Geology, v. 90, p. 1359–1380.

Wang, C.H., Song, Q.H., Wang, D.H., Li, L.X., Yu, C., Wang, Z.G., and Qu, W.J., 2009, Re-Os isotopic dating of molybdenite from the Daheishan molybdenum deposit of Jilin Province and its geological significance: Rock and Mineral Analysis, v. 28, p. 269–273 (in Chinese with English abstract).

Wang, J.P., Han, L., and Lv, K.P., 2011, Geological characteristics of the Chalukou molybdenum polymetallic deposit, Daxinganling: Mineral Resources and Geology, v. 25, p. 486–490 (in Chinese with English abstract).

Wang, G.R., Wu, G., Xu, L.Q., Li, X.Z., Liu, J., Zhang, T., Quan, Z.X., Wu, H., Li, T.G., and Chen, Y.C., 2017, Molybdenite Re-Os age, H-O-C-S-Pb isotopes, and fluid inclusion study of the Caosiyao porphyry Mo deposit in Inner Mongolia, China: Ore Geology Reviews, v. 81, p. 728–744.

Weis, P., Driesner, T., and Heinrich, C.A., 2012, Porphyry-copper ore shells form at stable pressure-temperature fronts within dynamic fluid plumes: Science, v. 338, p. 1613–1616.

Weis, P., 2015, The dynamic interplay between saline fluid flow and rock permeability in magmatic-hydrothermal systems: Geofluids, v. 15, p. 350–371.

Wilde, S.A., 2015, Final amalgamation of the Central Asian orogenic belt in NE China: Paleo-Asian Ocean closure versus Paleo-Pacific plate subduction—a review of the evidence: Tectonophysics, v. 662, p. 345–362.

Wiedenbeck, M., Alle, P., Corfu, F., Griffin, W.L., Meier, M., Oberli, F., Quadt, A.V., Roddick, J.C., and Spiegel, W., 1995, Three natural zircon standards for U-Th-Pb, Lu-Hf, trace element and REE analyses: Geostandards Newsletter, v. 19, p. 1–23.

Wu, F.Y., Lin, J.Q., Wilde, S.A., Zhang, X.O., and Yang, J.H., 2005, Nature and significance of the Early Cretaceous giant igneous event in eastern China: Earth and Planetary Science Letters, v. 233, p. 103–119.

Wu, F.Y., Sun, D.Y., Ge, W.C., Zhang, Y.B., Grant, M.L., Wilde, S.A., and Jahn, B.M., 2011,

Geochronology of the Phanerozoic granitoids in northeastern China: Journal of Asian Earth Sciences, v. 41, p. 1–30.

Xiong, S.F., He, M.C., Yao, S.Z., Cui, Y.B., Shi, G.Z., Ding, Z.J., and Hu, X.L., 2015, Fluid evolution of the Chalukou giant Mo deposit in the northern Great Xing'an Range, NE China: Geological Journal, v. 50, p. 720–738.

Yang, Z.M., and Cooke, D.R., 2019, Porphyry copper deposits in China, In: Mineral deposits of China, Society of Economic Geologists, Special Publication, Chang Zhaoshan, Goldfarb Richard J. (ed), United States, p. 133–187.

Zhai, D.G., Liu, J.J., Zhang, H.Y., Yao, M.J., Wang, J.P., and Yang, Y.Q., 2014, S-Pb isotopic geochemistry, U-Pb and Re-Os geochronology of the Huangganglianq Fe-Sn deposit, Inner Mongolia, NE China: Ore Geology Reviews, v. 59, p. 109–122.

Zhai, D.G., Liu, J.J, Zhang, A.L, and Sun, Y.Q, 2017, U-Pb, Re-Os and $^{40}Ar/^{39}Ar$ geochronology of porphyry Sn ± Cu ± Mo and polymetallic (Ag-Pb-Zn-Cu) vein mineralization at Bianjiadayuan, Inner Mongolia, NE China: Implications for discrete mineralization events: Economic Geology, v.1 12, p. 2041–2059.

Zhai, D.G., Williams-Jones, A.E., Liu, J.J., David, S., Li, C., Huang, X.W., Qi, L., and Guo, D.H., 2019a, Evaluating the use of the molybdenite Re-Os chronometer in dating gold mineralization: Evidence from the Haigou deposit, NE China: Economic Geology, v. 114, p. 897–915.

Zhai, D.G., Liu, J.J., Cook, N.J., Wang, X.L., Yang, Y.Q., Zhang, A.L., and Jiao Y.C., 2019b, Mineralogical, textural, sulfur and lead isotope constraints on the origin of Ag-Pb-Zn mineralization at Bianjiadayuan, Inner Mongolia, NE China: Mineralium Deposita, v. 54, p. 47–66.

Zhai, D.G., Williams-Jones, A.E., Liu, J.J., David, S., Voudouris, P.C., Tombros, S., Li, K., Li, P.L., and Sun, H., 2020, The genesis of the giant Shuangjianzishan epithermal Ag-Pb-Zn deposit, Inner Mongolia, northeastern China: Economic Geology, v. 115, p. 101–128.

Zhang, C., and Li, N., 2017, Geochronology and zircon Hf isotope geochemistry of granites in the giant Chalukou Mo deposit, NE China: Implications for tectonic setting: Ore Geology Reviews, v. 81, p. 780–793.

Zhou, J.B., Wilde, S.A., Zhao, G.C., and Han, J., 2018, Nature and assembly of microcontinental blocks within the Paleo-Asian Ocean: Earth-Science Reviews, v. 186, p. 76–93.

Zhou, L.L., Zeng, Q.D., Liu, J.M., Friis, H., Zhang, Z.L., Duan, X.X., and Lan, T.G., 2014, Geochronology of magmatism and mineralization of the Daheishan giant porphyry molybdenum deposit, Jilin Province, Northeast China: constraints on ore genesis and implications for geodynamic setting: International Geology Review, v. 56, p. 929–953.

Zimmerman, A., Stein, H.J., Morgan, J.W., Markey, R.J., and Watanabe, Y., 2014, Re-Os geochronology of the El Salvador porphyry Cu-Mo deposit, Chile: Tracking analytical improvements in accuracy and precision over the past decade: Geochimica et Cosmochimica Acta, v. 131, p. 13–32.

Figure captions

Fig. 1. The regional geology of the Chalukou porphyry Mo deposit in NE China. (A) Tectonic subdivisions of NE China (modified from Wu et al., 2011). (B) A geological map of NE China, showing the locations of major ore deposits (modified from Chen et al., 2017). The porphyry Mo deposits are classified as giant >500,000 tons, large 100,000-500,000 tons, medium 10,000-100,000 tons, and small <10,000 tons.

Fig. 2. (A) A geological map showing the main lithological units and faults in the Chalukou ore district (modified from Xiong et al., 2015). (B) A geological map of the Chalukou ore deposit (modified from Li et al., 2019).

Fig. 3. Cross sections of the Chalukou Mo deposit. (A) A cross section showing the location and crosscutting relationships of intrusions, dikes and hydrothermal breccias (modified from Li et al., 2014). (B) A cross section showing the distribution of the different hydrothermal alteration zones and orebodies (modified from Li et al., 2019).

Fig. 4. Photographs showing examples and crosscutting relationships of the various vein types. (A) A barren quartz vein ($A1_E$ vein) cut by a quartz-molybdenite vein ($B1_E$ vein) hosted in potassic granite porphyry. (B) A quartz ± molybdenite vein ($A2_E$ vein) cut by $A1_E$ veins. (C) $B1_E$ veins cut by an $A2_E$ vein. (D) Molybdenite-dominant quartz veins ($B2_E$ vein) cutting $A2_E$ and $A1_E$ veins. (E) Unidirectional solidification textures (USTs) cut by A_M veins and quartz-molybdenite veins ($B1_M$ veins). (F) Quartz-magnetite-hematite veins hosted in fine-grained porphyry. (G) $B1_M$ veins cut by a quartz-pyrite-fluorite vein (D_M vein). (H) A_M veins cut by D_M veins. (I) Vein breccia containing fragments of $B1_M$ veins and cemented by quartz and molybdenite. All the scale bars are 1 cm long.

Fig. 5. Photographs showing the characteristics of $B1_M$ and $B2_M$ veins. (A-B) Quartz-dominant $B1_M$

910 veins with linearly distributed molybdenite along the edges or in the suture. (C) A Mo-dominant
911 $B2_M$ vein cut by a later $B2_M$ vein. (D) A schematic diagram showing the proportion and distribution
912 of quartz and molybdenite in $B1_M$ and $B2_M$ veins.
913
914 Fig. 6. Zircon U-Pb concordia diagrams for the different igneous rocks in the Chalukou mine area.
915 (A) Granite porphyry. (B) Quartz porphyry. (C) Fine-grained porphyry. (D) Diorite porphyry. Also
916 show are the weighted mean ages and representative CL images of analysis zircon spots.
917
918 Fig. 7. Photographs showing the nature of the samples dated in this study and the corresponding Re-
919 Os ages. (A-C) $B1_E$, $A2_E$ and $B2_E$ veins, respectively, in the granite porphyry. (D-F) A_M and $B2_M$
920 veins, respectively, in the fine-grained porphyry. Abbreviations are same as in Table 1. All the scale
921 bars are 1 cm long.
922
923 Fig. 8. Summary of the ages for the main magmatic-hydrothermal events at Chalukou. (A)
924 Previously published ages of magmatism and mineralization at Chalukou. The red bars are from this
925 study. Data sources: 1 = Li et al. (2014), 2 = Duan et al. (2018), 3 = Zhang and Li (2017), 4 = Liu
926 et al. (2017), 5 = Nie et al. (2013), 6 = Liu et al. (2014b), 7 = Nie et al. (2011). (B) ID-N-TIMS
927 molybdenite Re-Os age determinations for the different veins investigated in this study. (C) A
928 summary of U-Pb and Re-Os age data for the Chalukou Mo porphyry deposit.
929
930 Fig. 9. A summary of data on the duration of ore-forming magmatic-hydrothermal activity for
931 selected porphyry type deposits. (A) A diagram showing the tonnage (Cu + Mo in millions of tons,
932 Mt) versus the duration of magmatism and mineralization (m.y.). (B) A diagram showing the
933 tonnage (Cu + Mo in million tons, Mt) versus age (Ma) of the deposits considered in A. The data
934 are from Bookstrom (1989), Long (1995), Wallace (1995), Anderson et al. (1998), Jensen (1998),
935 Selby and Creaser (2001), Barra et al. (2003), Dilles et al. (2003), Maksaev et al. (2004), Seedorff
936 and Einaudi (2004), Markey et al. (2007), Klemm et al. (2008), Sillitoe and Mortensen (2010), Li
937 et al. (2013), Stein (2014), Deckart et al. (2014), Zhou et al. (2014), Spencer et al. (2015), Buret et
938 al. (2016), Li et al. (2017b), and Chang et al. (2017).
939

940 Table 1. The textures, mineralogy, associated alteration and mode of occurrence of the different
941 vein-types observed in the Chalukou porphyry Mo deposit.
942
943 Table 2. Results of zircon LA-ICP-MS U-Pb chemical and isotopic analyses of the different igneous
944 rocks in the Chalukou deposit.
945
946 Table 3. Synopsis of molybdenite Re-Os isotope data from the Chalukou deposit.

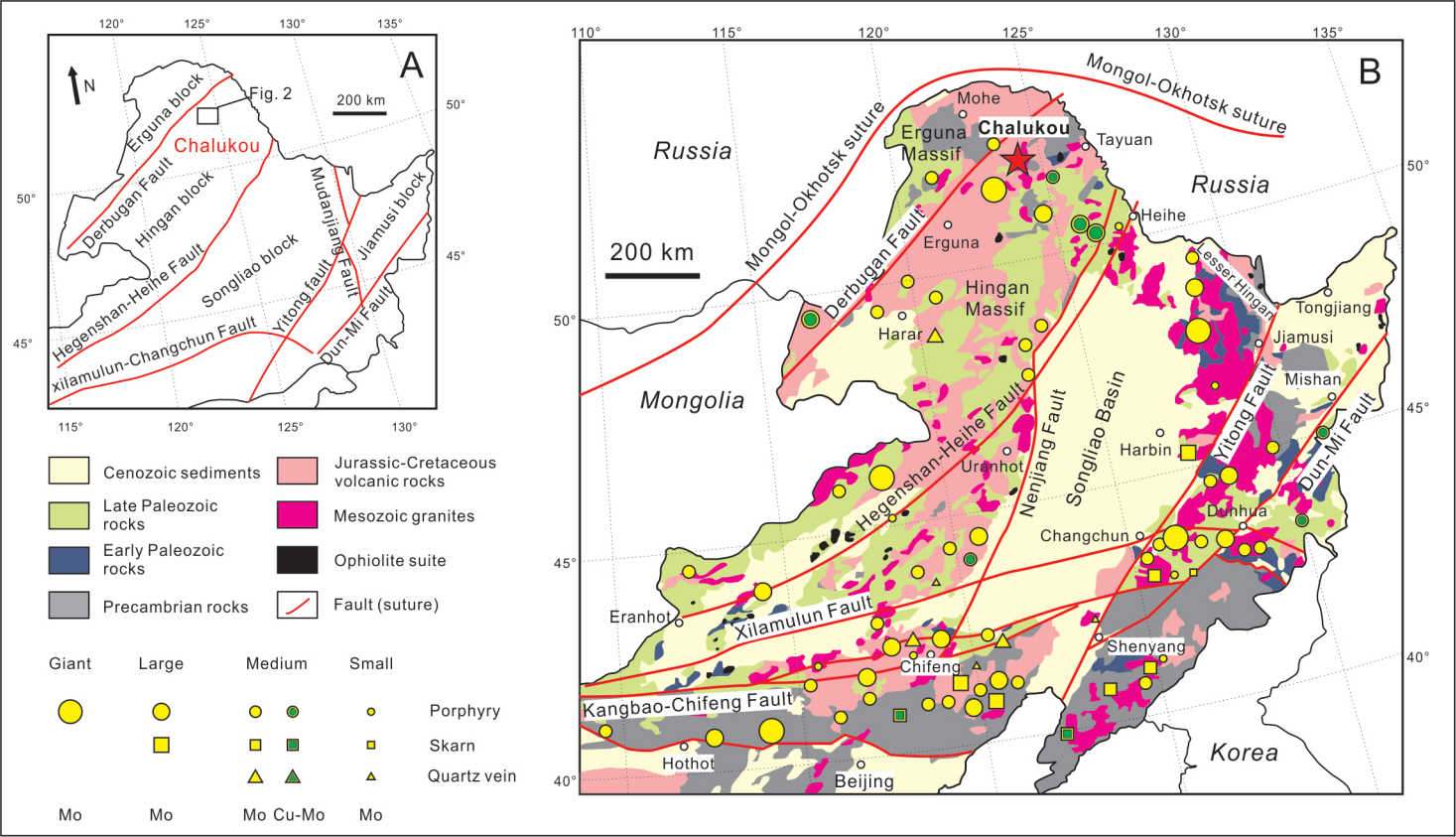
A
N
Fig. 2
200 km
Erguna block
Chalukou
Derbugan Fault
Hingan block
Hegenshan-Heihe Fault
Songliao block
Xilamulun-Changchun Fault
Yitong fault
Mudanjiang Fault
Jiamusi block
Dun-Mi Fault
120°
125°
130°
135°
50°
45°
115°
120°
125°
130°
Cenozoic sediments
Late Paleozoic rocks
Early Paleozoic rocks
Precambrian rocks
Jurassic-Cretaceous volcanic rocks
Mesozoic granites
Ophiolite suite
Fault (suture)
Giant
Large
Medium
Small
Porphyry
Skarn
Quartz vein
Mo
Mo
Mo
Cu-Mo
Mo
B
Mongol-Okhotsk suture
Mongol-Okhotsk suture
Russia
Russia
Mongolia
Korea
Mohe
Erguna Massif
Chalukou
Tayuan
Heihe
Erguna
200 km
Derbugan Fault
Hingan Massif
Lesser Hingan
Tongjiang
Harar
Jiamusi
Mishan
Hegenshan-Heihe Fault
Nenjiang Fault
Songliao Basin
Yitong Fault
Dun-Mi Fault
Harbin
Uranhot
Dunhua
Changchun
Eranhot
Xilamulun Fault
Shenyang
Chifeng
Kangbao-Chifeng Fault
Hothot
Beijing
110°
115°
120°
125°
130°
135°
50°
45°
40°

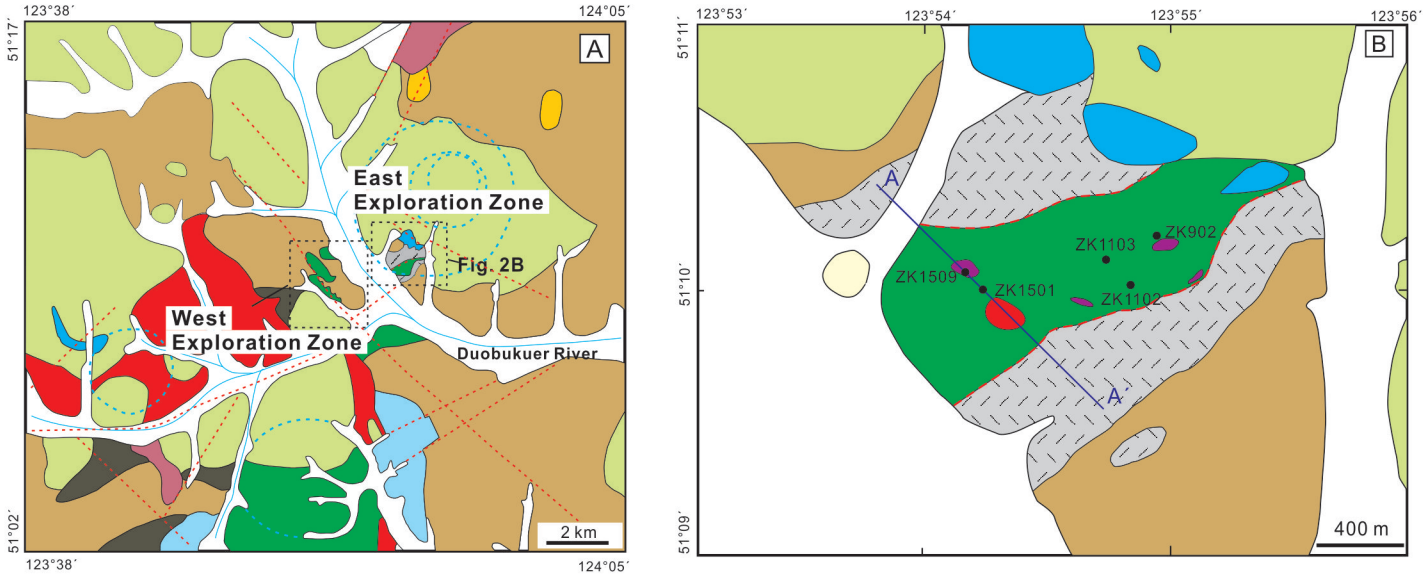
123°38′
124°05′
51°17′
51°02′
A
East
Exploration Zone
Fig. 2B
West
Exploration Zone
Duobukuer River
2 km
123°53′
123°54′
123°55′
123°56′
51°11′
51°10′
51°09′
B
A
A′
ZK1103
ZK902
ZK1509
ZK1501
ZK1102
400 m
Quaternary gravel
Neoproterozoic metamorphic rocks
Early Ordovician metavolcanic rocks
Metamorphic greywacke
Jurassic monzogranite
Jurassic granitie porphyry
Late Jurassic-Early Cretaceous rhyolite
Granite
Granodiorite
Creraceous quartz monzonite-porphyry
Quartz diorite
Breccia
Exploration Zones
Fault
Volcanic ring fracture
River
ZK1501
Sampling hole

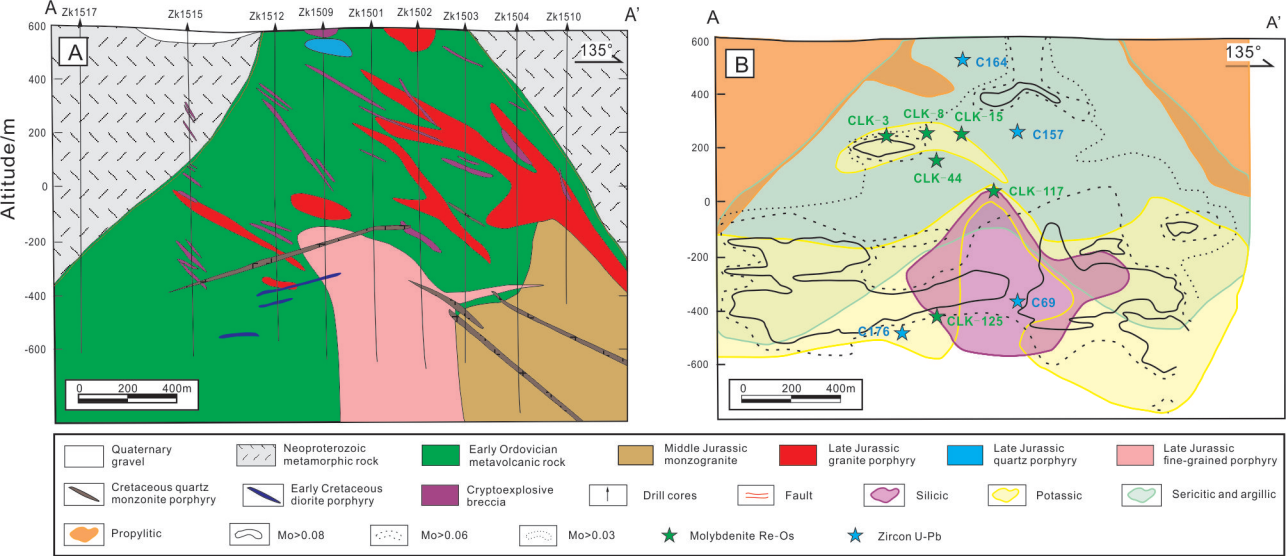
A
Zk1517
Zk1515
Zk1512
Zk1509
Zk1501
Zk1502
Zk1503
Zk1504
Zk1510
A'
A
135°
Altitude/m
600
400
200
0
-200
-400
-600
0 200 400m
B
C164
CLK-3
CLK-8
CLK-15
C157
CLK-44
CLK-117
C69
CLK-125
C176
Quaternary gravel
Neoproterozoic metamorphic rock
Early Ordovician metavolcanic rock
Middle Jurassic monzogranite
Late Jurassic granite porphyry
Late Jurassic quartz porphyry
Late Jurassic fine-grained porphyry
Cretaceous quartz monzonite porphyry
Early Cretaceous diorite porphyry
Cryptoexplosive breccia
Drill cores
Fault
Silicic
Potassic
Sericitic and argillic
Propylitic
Mo>0.08
Mo>0.06
Mo>0.03
Molybdenite Re-Os
Zircon U-Pb

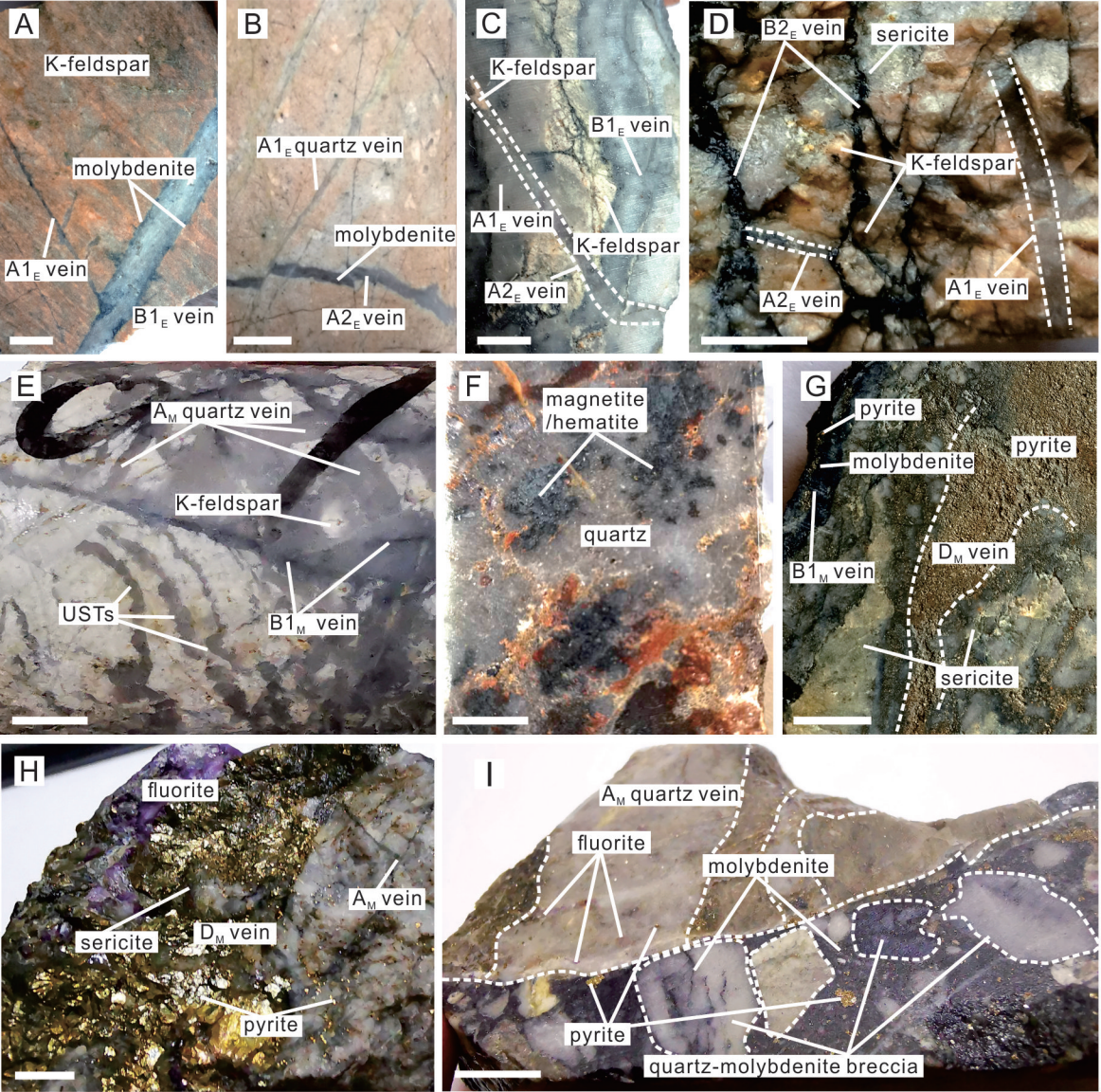
A
K-feldspar
molybdenite
A1E vein
B1E vein
B
A1E quartz vein
molybdenite
A2E vein
C
K-feldspar
B1E vein
A1E vein
K-feldspar
A2E vein
D
B2E vein
sericite
K-feldspar
A2E vein
A1E vein
E
AM quartz vein
K-feldspar
USTs
B1M vein
F
magnetite
/hematite
quartz
G
pyrite
pyrite
molybdenite
DM vein
B1M vein
sericite
H
fluorite
AM vein
sericite
DM vein
pyrite
I
AM quartz vein
fluorite
molybdenite
pyrite
quartz-molybdenite breccia

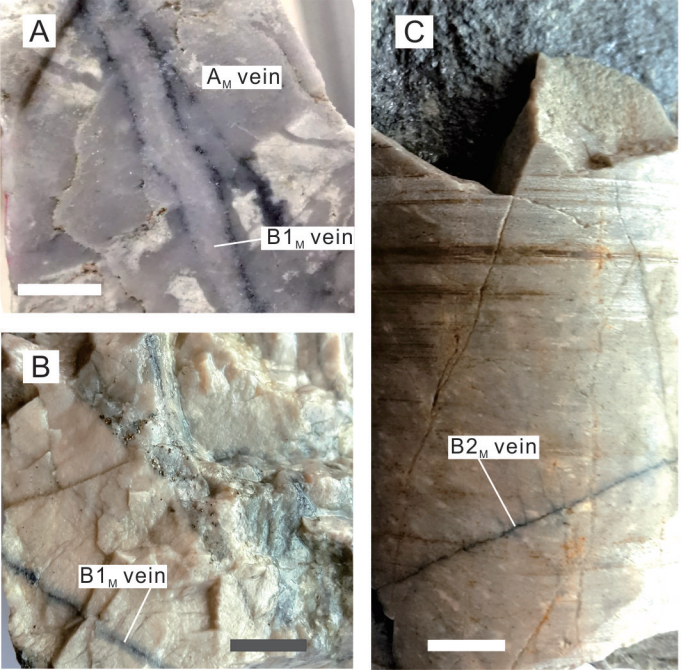
A
A_M vein
$B1_M$ vein
B
$B1_M$ vein
C
$B2_M$ vein
D
quartz
molybdenite
quartz
molybdenite
quartz
molybdenite
molybdenite
scale bar is 1 cm

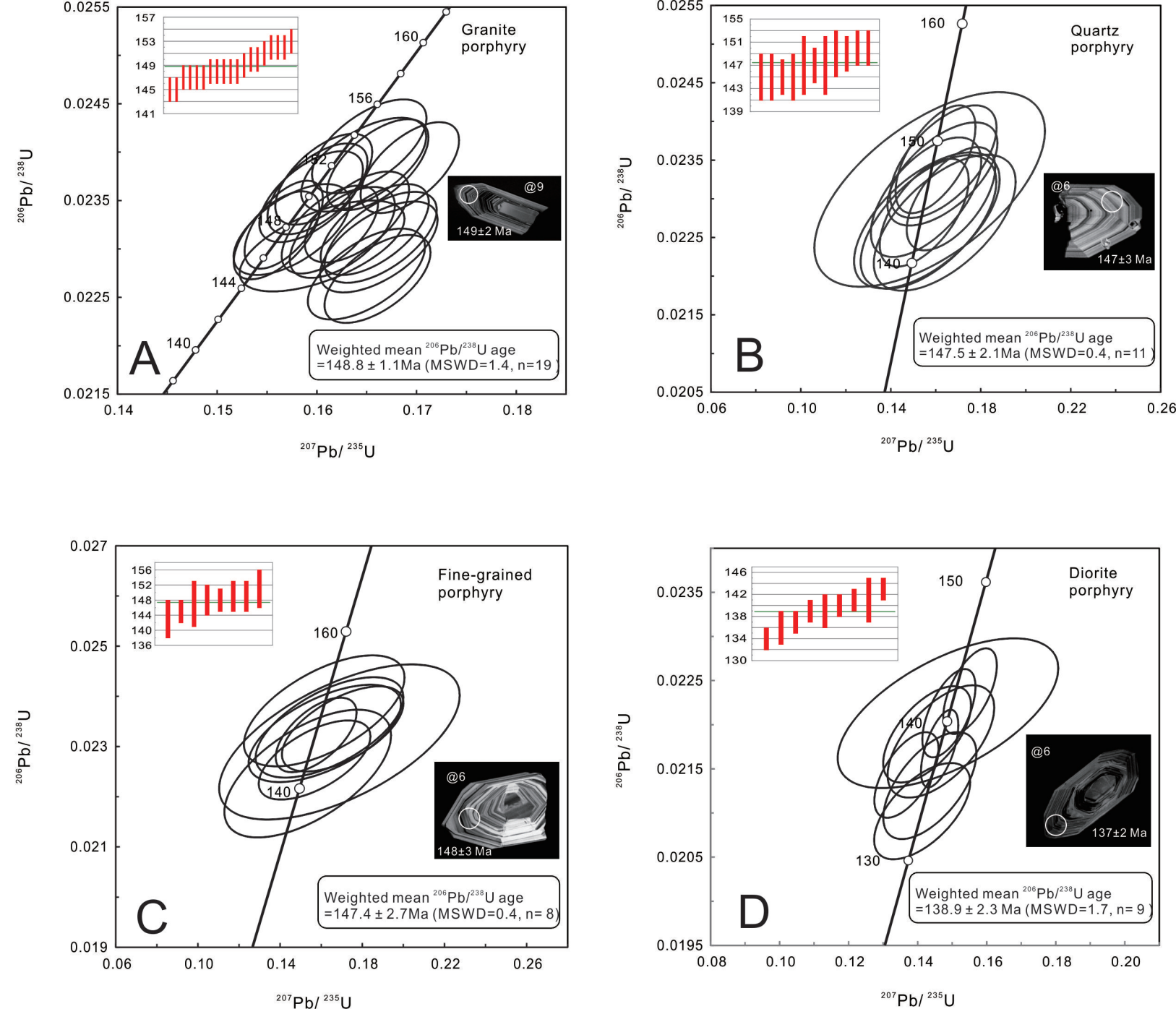
Granite porphyry
A
Weighted mean 206Pb/238U age =148.8 ± 1.1Ma (MSWD=1.4, n=19)
@9
149±2 Ma
Quartz porphyry
B
Weighted mean 206Pb/238U age =147.5 ± 2.1Ma (MSWD=0.4, n=11)
@6
147±3 Ma
Fine-grained porphyry
C
Weighted mean 206Pb/238U age =147.4 ± 2.7Ma (MSWD=0.4, n= 8)
@6
148±3 Ma
Diorite porphyry
D
Weighted mean 206Pb/238U age =138.9 ± 2.3 Ma (MSWD=1.7, n= 9)
@6
137±2 Ma
206Pb/238U
207Pb/235U

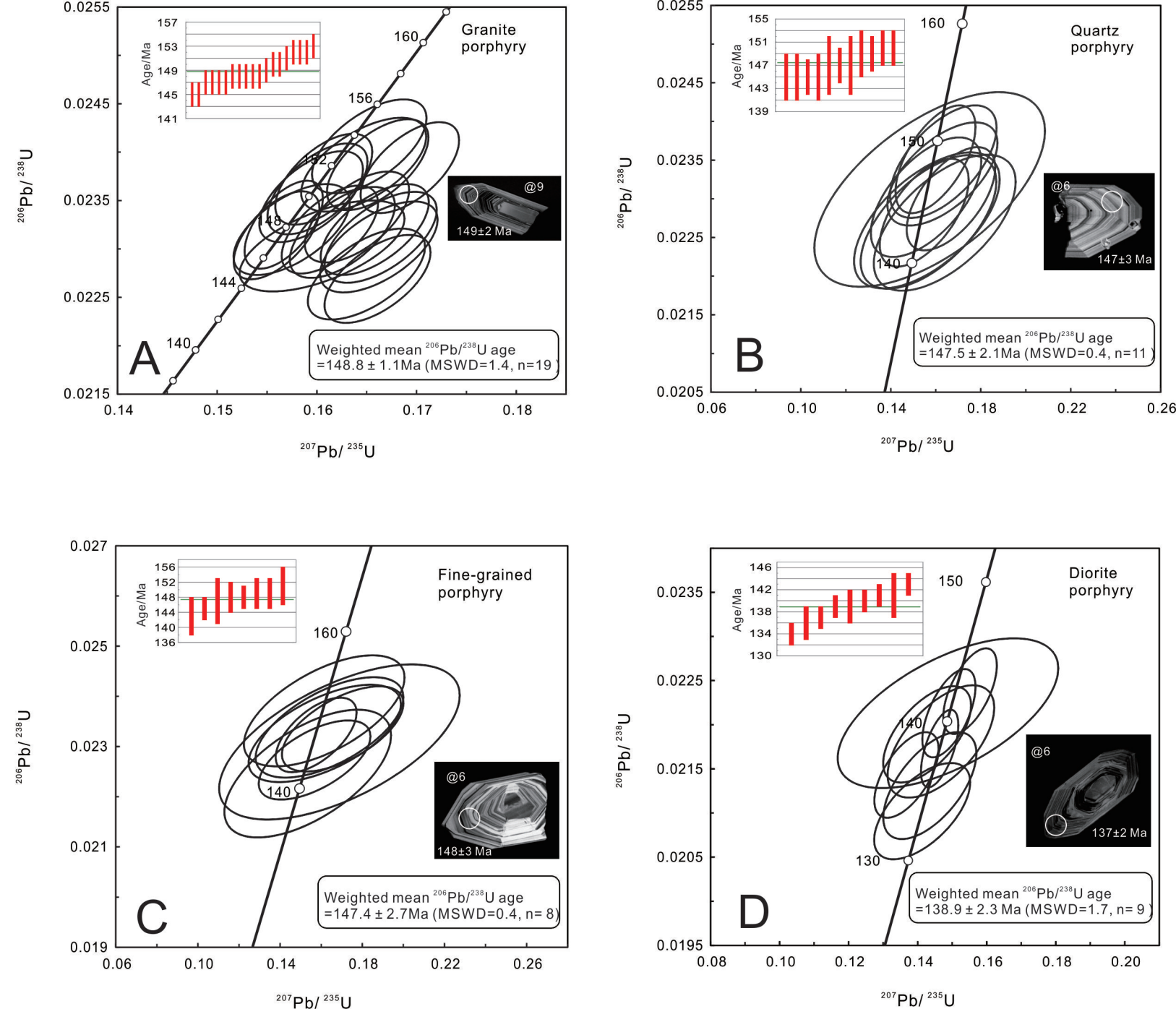
Granite porphyry
Age/Ma
157
153
149
145
141
160
156
152
148
144
140
@9
149±2 Ma
A
Weighted mean 206Pb/238U age
=148.8 ± 1.1Ma (MSWD=1.4, n=19)
206Pb/ 238U
207Pb/ 235U
0.0255
0.0245
0.0235
0.0225
0.0215
0.14
0.15
0.16
0.17
0.18
Quartz porphyry
Age/Ma
155
151
147
143
139
160
150
140
@6
147±3 Ma
B
Weighted mean 206Pb/238U age
=147.5 ± 2.1Ma (MSWD=0.4, n=11)
206Pb/ 238U
207Pb/ 235U
0.0255
0.0245
0.0235
0.0225
0.0215
0.0205
0.06
0.10
0.14
0.18
0.22
0.26
Fine-grained porphyry
Age/Ma
156
152
148
144
140
136
160
140
@6
148±3 Ma
C
Weighted mean 206Pb/238U age
=147.4 ± 2.7Ma (MSWD=0.4, n= 8)
206Pb/ 238U
207Pb/ 235U
0.027
0.025
0.023
0.021
0.019
0.06
0.10
0.14
0.18
0.22
0.26
Diorite porphyry
Age/Ma
146
142
138
134
130
150
140
130
@6
137±2 Ma
D
Weighted mean 206Pb/238U age
=138.9 ± 2.3 Ma (MSWD=1.7, n= 9)
206Pb/ 238U
207Pb/ 235U
0.0235
0.0225
0.0215
0.0205
0.0195
0.08
0.10
0.12
0.14
0.16
0.18
0.20

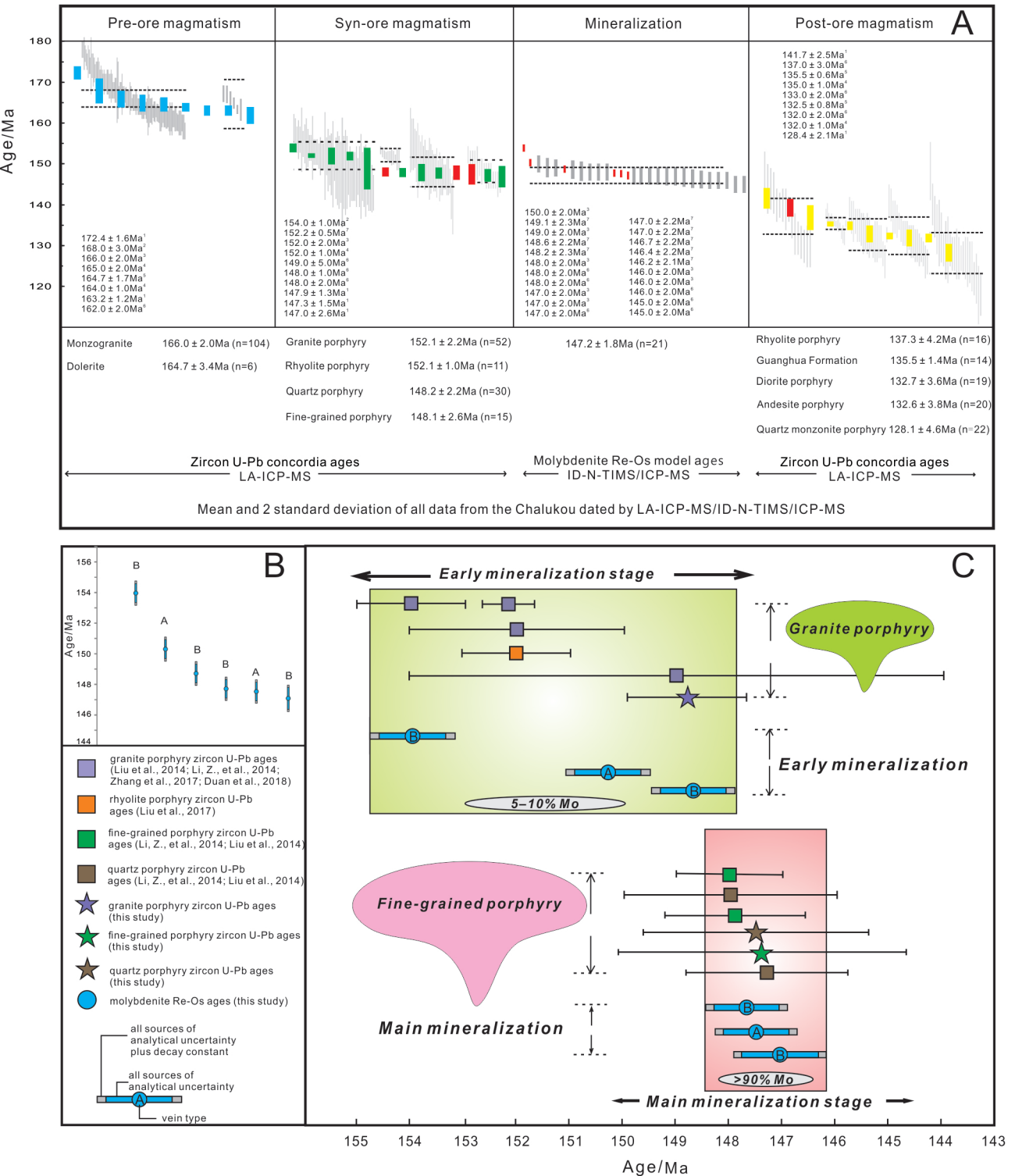
A
Pre-ore magmatism
Syn-ore magmatism
Mineralization
Post-ore magmatism
Age/Ma
180
170
160
150
140
130
120
172.4 ± 1.6Ma[1]
168.0 ± 3.0Ma[2]
166.0 ± 2.0Ma[3]
165.0 ± 2.0Ma[4]
164.7 ± 1.7Ma[5]
164.0 ± 1.0Ma[4]
163.2 ± 1.2Ma[1]
162.0 ± 2.0Ma[6]
154.0 ± 1.0Ma[2]
152.2 ± 0.5Ma[1]
152.0 ± 2.0Ma[3]
152.0 ± 1.0Ma[4]
149.0 ± 5.0Ma[4]
148.0 ± 1.0Ma[3]
148.0 ± 2.0Ma[4]
147.9 ± 1.3Ma[1]
147.3 ± 1.5Ma[1]
147.0 ± 2.6Ma[1]
150.0 ± 2.0Ma[3]
149.1 ± 2.3Ma[1]
149.0 ± 2.0Ma[4]
148.6 ± 2.2Ma[1]
148.2 ± 2.3Ma[1]
148.0 ± 2.0Ma[4]
148.0 ± 2.0Ma[3]
148.0 ± 2.0Ma[4]
147.0 ± 2.0Ma[3]
147.0 ± 2.0Ma[3]
147.0 ± 2.0Ma[6]
147.0 ± 2.2Ma[7]
147.0 ± 2.2Ma[7]
146.7 ± 2.2Ma[7]
146.4 ± 2.2Ma[7]
146.2 ± 2.1Ma[7]
146.0 ± 2.0Ma[3]
146.0 ± 2.0Ma[3]
146.0 ± 2.0Ma[8]
145.0 ± 2.0Ma[6]
145.0 ± 2.0Ma[6]
141.7 ± 2.5Ma[1]
137.0 ± 3.0Ma[6]
135.5 ± 0.6Ma[5]
135.0 ± 1.0Ma[4]
133.0 ± 2.0Ma[6]
132.5 ± 0.8Ma[5]
132.0 ± 2.0Ma[6]
132.0 ± 1.0Ma[4]
128.4 ± 2.1Ma[1]
Monzogranite 166.0 ± 2.0Ma (n=104)
Dolerite 164.7 ± 3.4Ma (n=6)
Granite porphyry 152.1 ± 2.2Ma (n=52)
Rhyolite porphyry 152.1 ± 1.0Ma (n=11)
Quartz porphyry 148.2 ± 2.2Ma (n=30)
Fine-grained porphyry 148.1 ± 2.6Ma (n=15)
147.2 ± 1.8Ma (n=21)
Rhyolite porphyry 137.3 ± 4.2Ma (n=16)
Guanghua Formation 135.5 ± 1.4Ma (n=14)
Diorite porphyry 132.7 ± 3.6Ma (n=19)
Andesite porphyry 132.6 ± 3.8Ma (n=20)
Quartz monzonite porphyry 128.1 ± 4.6Ma (n=22)
Zircon U-Pb concordia ages
LA-ICP-MS
Molybdenite Re-Os model ages
ID-N-TIMS/ICP-MS
Zircon U-Pb concordia ages
LA-ICP-MS
Mean and 2 standard deviation of all data from the Chalukou dated by LA-ICP-MS/ID-N-TIMS/ICP-MS
B
Age/Ma
156
154
152
150
148
146
144
B
A
B
B
A
B
granite porphyry zircon U-Pb ages (Liu et al., 2014; Li, Z., et al., 2014; Zhang et al., 2017; Duan et al., 2018)
rhyolite porphyry zircon U-Pb ages (Liu et al., 2017)
fine-grained porphyry zircon U-Pb ages (Li, Z., et al., 2014; Liu et al., 2014)
quartz porphyry zircon U-Pb ages (Li, Z., et al., 2014; Liu et al., 2014)
granite porphyry zircon U-Pb ages (this study)
fine-grained porphyry zircon U-Pb ages (this study)
quartz porphyry zircon U-Pb ages (this study)
molybdenite Re-Os ages (this study)
all sources of analytical uncertainty plus decay constant
all sources of analytical uncertainty
A
vein type
C
Early mineralization stage
Granite porphyry
Early mineralization
B
A
B
5–10% Mo
Fine-grained porphyry
Main mineralization
B
A
B
>90% Mo
Main mineralization stage
155
154
153
152
151
150
149
148
147
146
145
144
143
Age/Ma

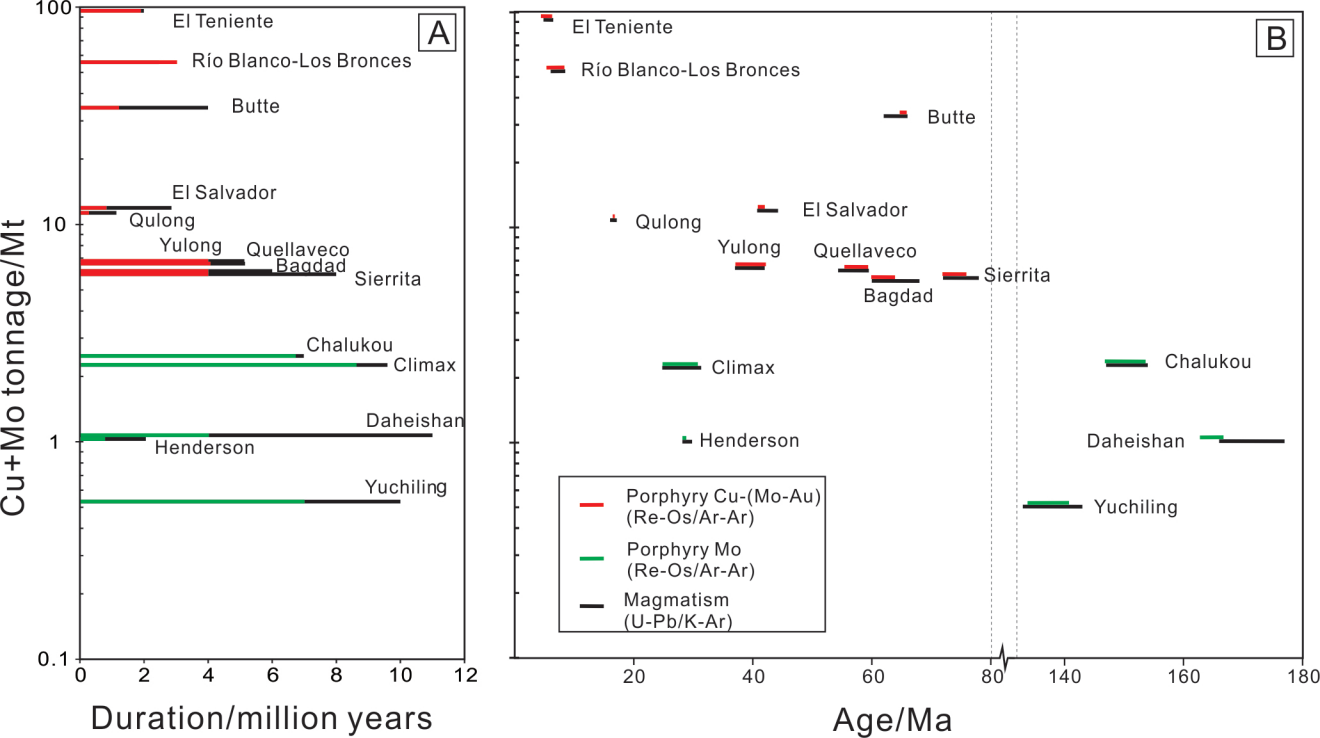
A
B
Cu+Mo tonnage/Mt
100
10
1
0.1
El Teniente
Río Blanco-Los Bronces
Butte
El Salvador
Qulong
Yulong
Quellaveco
Bagdad
Sierrita
Chalukou
Climax
Daheishan
Henderson
Yuchiling
0
2
4
6
8
10
12
Duration/million years
20
40
60
80
140
160
180
Age/Ma
Porphyry Cu-(Mo-Au)
(Re-Os/Ar-Ar)
Porphyry Mo
(Re-Os/Ar-Ar)
Magmatism
(U-Pb/K-Ar)

Table 1. The textures, mineralogy, associated alteration and mode of occurrence of the different vein-types observed in the Chalukou porphyry Mo deposit.

Types	Vein textures	Mineralogy	Alteration	Occurrences
Early period				
$A1_E$	Barren quartz vein (0.5-3 mm); irregular or straight walls	qtz, kfs	-	Occurring within granite porphyry and felsic-intermediate volcanic-sedimentary rocks; cut by other veins
$B1_E$	Thin qtz-mo veins (2-10 mm); mo abundant at vein margins	qtz, mo, py, kfs	kfs halos	Dominant vein-type in the shallow granite porphyry, rarely observed within the breccia; cuts $A1_E$ veins, cut by $A2_E$ veins
$A2_E$	Straight walls with minor mo (1-5 mm)	qtz, mo, py	kfs halos	Observed at shallow level associated with the granite porphyry; cuts $B1_E$ veins
$B2_E$	Mo dominant-veins with minor quartz; straight walls (1-3 mm)	mo, qtz, ser	ser halos	Commonly observed within the granite porphyry in dense stockworks; rarely observed mo-ser veins; most abundant mo-bearing vein type; cuts $A1_E$ and $A2_E$ veins
Main period				
UST	Thin sinuous quartz veins (2-6 mm)	qtz, kfs	-	Occurring at depth (>800 m) at the apex of the fine-grained porphyry; cut by A_M and $B1_M$ veins
A_M	Quartz veins with irregular or straight walls (1-15 mm)	qtz, mt, hem, py, fl, kfs	kfs halos	Occurring at depth associated with fine-grained porphyry; cuts USTs, cut by $B1_M$ and $B2_M$ veins
$B1_M$	Qtz-mo veins (2-10 mm) with straight walls;	qtz, mo, py	kfs halos	Most commonly observed within the fine-grained porphyry and volcanic-sedimentary rocks; cuts A_M veins
$B2_M$	Fine mo veins (1-5 mm); more mo than qtz in veins	mo, py, qtz, kfs	kfs halos	Frequently observed in the fine-grained porphyry at depths up to 1200 m; cuts A_M veins
D_M	Qtz-py veins with straight walls (5-40 mm); euhedral py intergrown with fl	py, mo, cp, gn, sph, qtz, ser, fl	ser halos	Commonly developed; cuts all the above veins

Abbreviations: cp = chalcopyrite, fl = fluorite, gn = galena, hem= hematite, kfs = K-feldspar, mo = molybdenite, mt = magnetite, py = pyrite, qtz = quartz, ser = sericite, sph = sphalerite

Table 2. Results of zircon LA-ICP-MS U-Pb chemical and isotopic analyses of the different igneous rocks in the Chalukou deposit

	Concentrations (ppm)				Isotopic ratios						Ages (Ma)					
Spot	Th	U	Pb	Th/U	$^{207}Pb/^{206}Pb$	1σ	$^{207}Pb/^{235}U$	1σ	$^{206}Pb/^{238}U$	1σ	$^{207}Pb/^{206}Pb$	1σ	$^{207}Pb/^{235}U$	1σ	$^{206}Pb/^{238}U$	1σ
Granite porphyry																
C157-01	213.2	367.1	9.9	0.58	0.0492	0.0012	0.1575	0.0039	0.0232	0.0003	159	33	148	3	148	2
C157-02	363.9	459.2	12.9	0.79	0.0526	0.0013	0.1650	0.0039	0.0227	0.0003	312	30	155	3	145	2
C157-03	479.3	436.1	13.0	1.10	0.0524	0.0013	0.1662	0.0039	0.0230	0.0003	301	30	156	3	147	2
C157-04	479.6	538.3	15.1	0.89	0.0531	0.0012	0.1661	0.0035	0.0227	0.0003	332	25	156	3	145	2
C157-05	643.0	713.3	20.4	0.90	0.0489	0.0008	0.1567	0.0026	0.0233	0.0003	142	18	148	2	148	2
C157-06	458.6	490.8	14.2	0.93	0.0509	0.0011	0.1626	0.0035	0.0232	0.0003	234	26	153	3	148	2
C157-07	281.8	469.9	12.9	0.60	0.0518	0.0012	0.1658	0.0036	0.0232	0.0003	278	26	156	3	148	2
C157-08	317.2	584.3	15.6	0.54	0.0504	0.0010	0.1613	0.0032	0.0232	0.0003	214	23	152	3	148	2
C157-09	533.3	459.0	13.9	1.16	0.0510	0.0011	0.1640	0.0035	0.0233	0.0003	240	25	154	3	149	2
C157-10	596.9	749.5	21.7	0.80	0.0515	0.0010	0.1693	0.0033	0.0238	0.0003	264	22	159	3	152	2
C157-11	569.9	597.7	17.2	0.95	0.0489	0.0009	0.1560	0.0028	0.0231	0.0003	142	21	147	2	147	2
C157-12	331.0	445.1	12.5	0.74	0.0522	0.0012	0.1664	0.0037	0.0231	0.0003	293	28	156	3	147	2
C157-13	305.4	355.9	10.5	0.86	0.0500	0.0013	0.1647	0.0041	0.0239	0.0003	197	34	155	4	152	2
C157-14	403.9	512.4	14.6	0.79	0.0491	0.0011	0.1594	0.0034	0.0235	0.0003	154	27	150	3	150	2
C157-15	376.8	458.8	13.2	0.82	0.0491	0.0011	0.1601	0.0033	0.0236	0.0003	155	25	151	3	150	2
C157-16	346.6	401.9	12.0	0.86	0.0498	0.0012	0.1653	0.0038	0.0241	0.0003	186	30	155	3	153	2
C157-17	370.7	844.4	22.8	0.44	0.0505	0.0019	0.1605	0.0055	0.0230	0.0003	220	87	151	5	147	2
C157-18	496.7	533.6	15.9	0.93	0.0505	0.0011	0.1661	0.0034	0.0239	0.0003	216	24	156	3	152	2
C157-19	326.6	527.9	14.8	0.62	0.0491	0.0010	0.1607	0.0032	0.0237	0.0003	154	24	151	3	151	2

Table 2. (Cont.)

Spot	Concentrations (ppm)			Th/U	Isotopic ratios						Ages (Ma)					
	Th	U	Pb		$^{207}Pb/^{206}Pb$	1σ	$^{207}Pb/^{235}U$	1σ	$^{206}Pb/^{238}U$	1σ	$^{207}Pb/^{206}Pb$	1σ	$^{207}Pb/^{235}U$	1σ	$^{206}Pb/^{238}U$	1σ
Quartz porphyry																
C164-01	81.7	105.8	3.0	0.77	0.0496	0.0087	0.1581	0.0273	0.0231	0.0007	178	291	149	24	147	5
C164-02	98.2	106.1	3.2	0.93	0.0505	0.0068	0.1576	0.0210	0.0227	0.0006	216	248	149	18	145	4
C164-03	115.2	142.0	5.2	0.81	0.0505	0.0074	0.1622	0.0233	0.0233	0.0007	218	265	153	20	149	4
C164-04	99.2	87.7	2.8	1.13	0.0507	0.0051	0.1630	0.0161	0.0233	0.0004	228	189	153	14	149	3
C164-05	144.5	115.1	3.9	1.25	0.0494	0.0037	0.1599	0.0117	0.0235	0.0005	165	129	151	10	150	3
C164-06	81.9	76.6	2.4	1.07	0.0491	0.0052	0.1557	0.0162	0.0230	0.0005	152	192	147	14	147	3
C164-07	943.6	362.2	15.4	2.61	0.0505	0.0049	0.1634	0.0156	0.0235	0.0005	218	178	154	14	150	3
C164-08	735.7	749.8	29.0	0.98	0.0501	0.0065	0.1568	0.0199	0.0227	0.0006	201	236	148	17	145	4
C164-09	139.6	128.7	4.1	1.08	0.0493	0.0042	0.1549	0.0131	0.0228	0.0005	160	152	146	11	145	3
C164-10	55.1	59.2	1.8	0.93	0.0494	0.0107	0.1573	0.0338	0.0231	0.0008	166	340	148	30	147	5
C164-11	51.8	95.4	2.8	0.54	0.0524	0.0068	0.1640	0.0208	0.0227	0.0006	305	239	154	18	145	4
Fine-grained porphyry																
C69-01	105.9	86.9	2.9	1.22	0.0505	0.0077	0.1618	0.0245	0.0233	0.0006	216	277	152	21	148	4
C69-02	84.3	88.5	2.7	0.95	0.0501	0.0058	0.1568	0.0180	0.0227	0.0005	198	215	148	16	145	3
C69-03	98.6	117.6	3.6	0.84	0.0509	0.0075	0.1641	0.0237	0.0234	0.0007	237	270	154	21	149	4
C69-04	67.0	74.6	2.3	0.90	0.0531	0.0123	0.1689	0.0387	0.0231	0.0010	332	375	158	34	147	6
C69-05	53.8	57.3	1.8	0.94	0.0530	0.0062	0.1705	0.0195	0.0234	0.0006	328	214	160	17	149	4
C69-06	153.7	114.3	3.7	1.34	0.0492	0.0041	0.1576	0.0130	0.0232	0.0005	158	146	149	11	148	3
C69-07	66.6	74.1	2.2	0.90	0.0496	0.0088	0.1535	0.0268	0.0225	0.0008	176	290	145	24	143	5
C69-08	210.8	131.8	4.5	1.60	0.0494	0.0080	0.1615	0.0258	0.0237	0.0007	168	274	152	23	151	5

Table 2. (Cont.)

Spot	Concentrations (ppm)			Th/U	Isotopic ratios						Ages (Ma)					
	Th	U	Pb		$^{207}Pb/^{206}Pb$	1σ	$^{207}Pb/^{235}U$	1σ	$^{206}Pb/^{238}U$	1σ	$^{207}Pb/^{206}Pb$	1σ	$^{207}Pb/^{235}U$	1σ	$^{206}Pb/^{238}U$	1σ
Diorite porphyry																
C176-01	71.3	61.4	1.7	1.16	0.0489	0.0031	0.1435	0.0089	0.0213	0.0004	141	105	136	8	136	3
C176-02	143.7	92.2	2.7	1.56	0.0487	0.0032	0.1413	0.0092	0.0210	0.0004	135	114	134	8	134	2
C176-03	140.6	348.2	8.6	0.40	0.0489	0.0012	0.1464	0.0036	0.0217	0.0003	141	33	139	3	139	2
C176-04	55.5	148.5	3.9	0.37	0.0473	0.0029	0.1428	0.0084	0.0219	0.0004	64	135	135	7	140	2
C176-05	93.1	61.4	1.9	1.52	0.0488	0.0035	0.1468	0.0102	0.0218	0.0004	138	120	139	9	139	3
C176-06	238.8	403.3	10.4	0.59	0.0463	0.0022	0.1368	0.0061	0.0214	0.0003	13	102	130	5	137	2
C176-07	96.6	245.1	6.1	0.39	0.0489	0.0017	0.1491	0.0051	0.0221	0.0003	141	52	141	4	141	2
C176-08	45.0	33.1	1.4	1.36	0.0488	0.0070	0.1488	0.0211	0.0221	0.0006	136	253	141	19	141	4
C176-09	125.3	225.9	6.0	0.55	0.0503	0.0017	0.1552	0.0051	0.0224	0.0003	208	50	146	5	143	2

Table 3. Results of Re-Os isotopic analyses of molybdenite samples from the Chalukou deposit

Sample No.	Location	Vein type	Alteration	Weight (g)	Re (ppm)	±	^{187}Re (ppm)	±	^{187}Os (ppb)	±	Model age (Ma)	±^	±*	±$^{\#}$
16CLK-3	320m/CM9	$B1_E$	potassic	0.02	39.71	0.14	24.96	0.09	64.10	0.19	153.96	0.08	0.63	0.79
16CLK-8	320m/CM7	$A2_E$	potassic	0.02	45.22	0.17	28.42	0.11	71.24	0.23	150.28	0.06	0.62	0.78
16CLK-15	320m/CM9	$B2_E$	sericitic	0.03	25.87	0.09	16.26	0.06	40.33	0.12	148.67	0.07	0.62	0.77
16CLK-44	567m/ZK1102	$B2_M$	potassic	0.02	43.60	0.16	27.41	0.10	67.51	0.21	147.67	0.10	0.60	0.76
16CLK-117	1085m/ZK1103	$B2_M$	sericitic	0.03	4.21	0.02	2.64	0.01	6.48	0.02	147.04	0.12	0.72	0.86
16CLK-125	419m/ZK1509	A_M	potassic	0.02	30.06	0.11	18.89	0.07	46.48	0.15	147.49	0.09	0.60	0.76

Notes: ^uncertainty including only mass spectrometry uncertainty

*uncertainty including all sources of analytical uncertainty

$^{\#}$uncertainty including all sources of analytical uncertainty plus decay constant